

TLM-21

DSN Telemetry System, Block-V Receiver

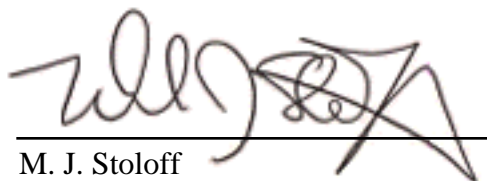
December 1, 1996

Prepared by:



P. W. Kinman
Cognizant Development Engineer

Approved by:



M. J. Stoloff
DSN System Engineer

Released by:



DSN Document Release

1. Introduction

1.1 Purpose

This module describes the capabilities of the Block-V Receiver as installed at the Deep Space Communications Complexes (DSCCs). It is intended to provide sufficient information to enable telecommunications engineers to predict telemetry performance when using the Block-V Receiver.

1.2 Scope

The scope of this module is limited to those features of the Block-V Receiver that have a direct effect upon telemetry performance.

1.3 *Contents*

| | | |
|-----------------------|-------------------------------------------------------|----|
| 1. | Introduction | 1 |
| 1.1 | Purpose | 1 |
| 1.2 | Scope | 1 |
| 1.3 | Contents | 2 |
| 2. | General Information | 4 |
| 2.1 | Telemetry Capability | 4 |
| 2.1.1 | Modulation | 6 |
| 2.1.2 | Symbol Rate | 7 |
| 2.1.3 | Carrier Loop Bandwidth | 7 |
| 2.2 | Definitions | 8 |
| 2.3 | Receiver Acquisition | 10 |
| 2.3.1 | FFT | 10 |
| 2.3.2 | Loop Locking | 15 |
| 2.3.3 | Acquisition Time | 16 |
| 2.4 | Telemetry Performance | 22 |
| 2.4.1 | Comparison of Residual Carrier and Suppressed Carrier | 23 |
| 2.4.2 | Decoding Threshold and System Loss | 25 |
| 2.4.3 | Carrier Synchronization | 27 |
| 2.4.3.1 | Residual Carrier | 27 |
| 2.4.3.2 | Suppressed Carrier | 40 |
| 2.4.3.3 | Two-Way Coherent | 41 |
| 2.4.4 | Subcarrier Synchronization | 45 |
| 2.4.5 | Symbol Synchronization | 47 |
| 2.4.6 | Waveform Distortion | 52 |
| Appendices | | |
| Appendix A | Ideal Functional Dependence of BER on E_b/N_0 | 54 |
| Appendix B | Radio Loss | 55 |
| Appendix C | Static Phase Error | 59 |
| Appendix D | Transmitter Phase Noise | 60 |
| Appendix E | Solar Phase Noise | 61 |
| Appendix F | Subcarrier Demodulation Loss | 62 |
| Appendix G | Symbol Loop Squaring Loss | 65 |
| Appendix H | Symbol Synchronization Loss | 65 |
| Appendix I | References | 66 |

Figures

| | | |
|-----------|----------------------------------------------------------------------|----|
| Figure 1 | Block-V Receiver Architecture | 5 |
| Figure 2 | Number of Data Points for FFT; Sample Rate = 2000 Hz | 13 |
| Figure 3 | Number of Data Points for FFT; Sample Rate = 20 Hz | 14 |
| Figure 4 | Loop Locking Time | 18 |
| Figure 5 | Receiver Acquisition Time; Residual Carrier | 19 |
| Figure 6 | Receiver Acquisition Time; Suppressed Carrier | 20 |
| Figure 7 | Receiver Acquisition Time; Suppressed Carrier | 21 |
| Figure 8 | Comparison of Residual Carrier and Suppressed Carrier | 24 |
| Figure 9 | Comparison of Optimized and Nonoptimized Mod. Index | 26 |
| Figure 10 | Telemetry Performance; Uncoded, Residual | 29 |
| Figure 11 | Telemetry Performance; ($k = 7, r = 1/2$), Residual | 30 |
| Figure 12 | Telemetry Performance; ($k = 15, r = 1/4$), Residual | 31 |
| Figure 13 | Telemetry Performance; ($k = 15, r = 1/6$), Residual | 32 |
| Figure 14 | Optimum Modulation Index; Uncoded | 33 |
| Figure 15 | Optimum Modulation Index; ($k = 7, r = 1/2$) | 34 |
| Figure 16 | Optimum Modulation Index; ($k = 15, r = 1/4$) | 35 |
| Figure 17 | Radio Loss (HRM); Uncoded, Residual | 37 |
| Figure 18 | Radio Loss (HRM); ($k = 7, r = 1/2$), Residual | 38 |
| Figure 19 | Radio Loss (HRM); ($k = 15, r = 1/4$), Residual | 39 |
| Figure 20 | Radio Loss (HRM); Uncoded, Suppressed | 42 |
| Figure 21 | Radio Loss (HRM); ($k = 7, r = 1/2$), Suppressed | 43 |
| Figure 22 | Radio Loss (HRM); ($k = 15, r = 1/4$), Suppressed | 44 |
| Figure 23 | Two-Way Radio Loss (HRM); Residual, X-up/X-down | 46 |
| Figure 24 | Squarewave Subcarrier Demodulation Loss; Uncoded | 48 |
| Figure 25 | Squarewave Subcarrier Demodulation Loss; ($k = 7, r = 1/2$) | 49 |
| Figure 26 | Squarewave Subcarrier Demodulation Loss; ($k = 15, r = 1/4$) | 50 |
| Figure 27 | Symbol Loop Squaring Loss | 51 |
| Figure 28 | Symbol Synchronization Loss | 53 |

Tables

| | | |
|-----------|----------------------------------------------------------------------------------|----|
| Table 1 | Telemetry Capabilities of the Block-V Receiver | 6 |
| Table 2 | Symbol Rates With the Block-V Receiver | 6 |
| Table 3 | FFT Sample Frequencies | 11 |
| Table 4 | FFT Section Bandwidths | 11 |
| Table 5 | Coefficients α_1 and α_2 in the Calculation of P_{CTP}/N_0 | 15 |
| Table 6 | Effective Threshold Energy per Bit to Noise Density Ratio | 25 |
| Table A-1 | Coefficients a_0 and a_1 for Equation (A-4) | 54 |
| Table B-1 | HRM Radio Loss | 58 |
| Table B-2 | LRM Radio Loss | 57 |
| Table C-1 | Static Phase Error for Block-V Receiver | 60 |
| Table D-1 | Carrier Phase Error Variance | 61 |
| Table F-1 | Squarewave Subcarrier Demodulation Loss | 63 |
| Table F-2 | Sinewave Subcarrier Demodulation Loss | 64 |

2. *General Information*

Figure 1 shows the architecture of the Block-V Receiver. At the front of the receiver are multiple stages of analog downconversion. The hardware used within these stages depends on the band in which the downlink is operating. The local oscillators remain at a constant setting for the duration of a tracking pass. The channel-select synthesizer is adjusted before the beginning of a pass to a value appropriate for the channel (within the band) of the incoming downlink signal. The anti-aliasing filter is a necessary precursor to sampling, and the Automatic Gain Control (AGC) is a necessary precursor to quantization. Carrier, subcarrier and symbol synchronization are all performed digitally within the digital demodulator (Reference 1). Doppler compensation is also done within the digital demodulator. The output of the receiver is a stream of soft-quantized symbols, suitable for input to a decoder.

The Block-V Receiver differs markedly from the earlier analog receivers, the Block III and Block IV, in a number of important respects. The Block-V Receiver incorporates much of the functionality of the Baseband Assembly (namely, subcarrier demodulation and symbol synchronization and detection) so that the output of this receiver will ordinarily interface directly with a decoder. (When an array of antennas is used, however, there will be a combiner between the receivers and the decoder.) Furthermore, the Block-V Receiver can track either a residual carrier or a suppressed carrier, the latter by use of a Costas loop (Reference 2).

Since the feedback loops (carrier, subcarrier, and symbol) of the Block-V Receiver are completely digital with loop filters implemented in software, loop bandwidths can be freely chosen by the user from a continuum of possible values. Moreover, loop bandwidths can be changed during a tracking pass without losing phase-lock. This flexibility in the selection and change of loop bandwidth obviates the kind of coarse bandwidth adaptivity that was built into the analog receivers. (The Block-III and Block-IV Receivers were designed with bandpass limiters preceding the final carrier phase detector, causing carrier loop bandwidth to vary with signal level.)

The Block-V Receiver offers the prospect of using very small carrier loop bandwidths. This is made possible by two elements of this receiver's design. The carrier loop is closed at an intermediate-frequency stage, which reduces the amount of frequency multiplication required within the loop; and the loop closure is digital, which makes the loop parameters numeric. These design elements ensure loop stability that is much superior to that of the analog receivers. As a result, the narrowest carrier loop bandwidth that can be used with the Block-V Receiver is limited only by the inherent stability of the incoming carrier and by the amount of uncompensated Doppler dynamics present.

2.1 *Telemetry Capability*

Table 1 shows the types of telemetry signals that can be tracked by the Block-V Receiver. Table 2 shows the symbol rates that can be tracked.

Figure 1: Block-V Receiver Architecture

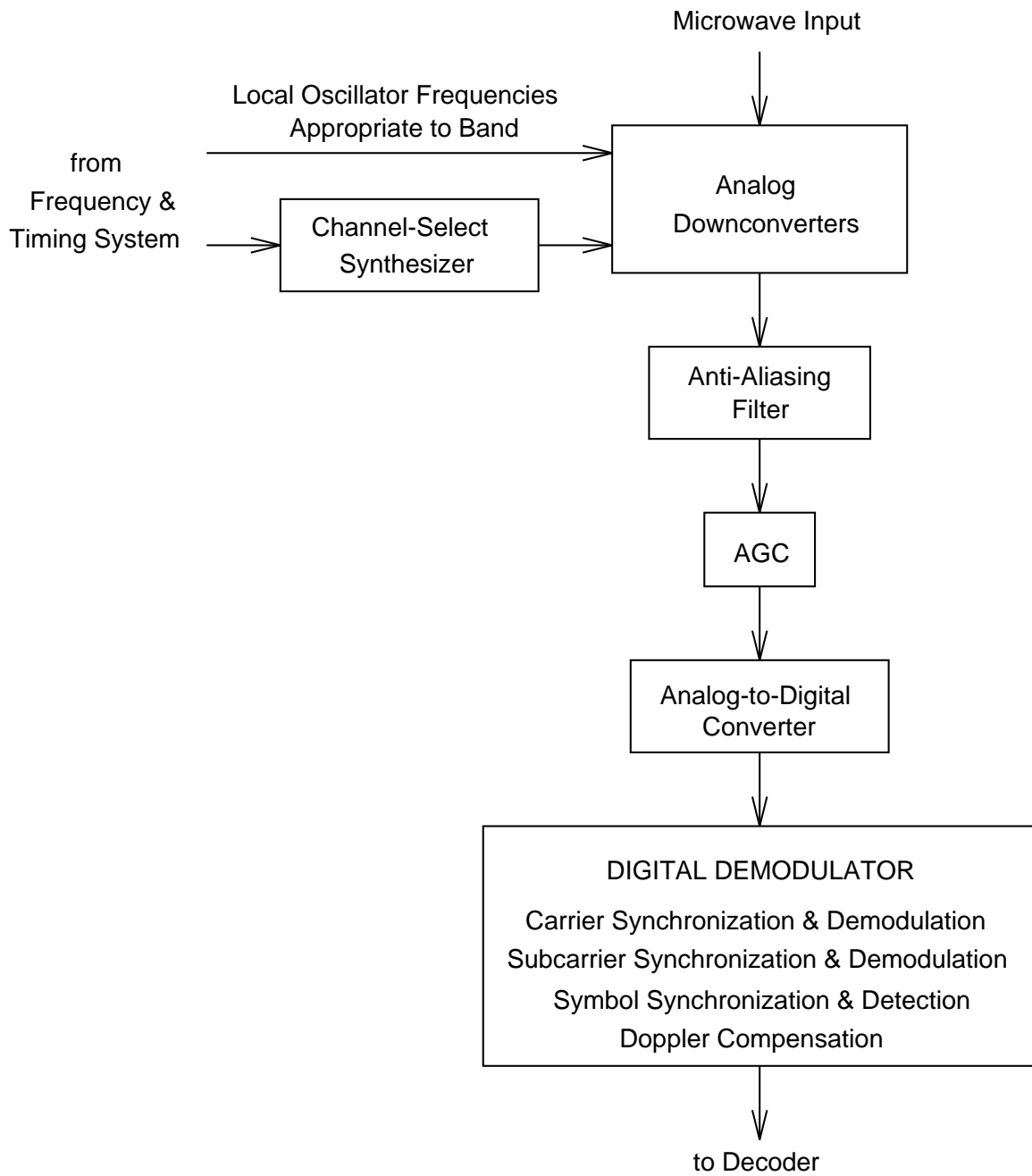


Table 1: Telemetry Capabilities of the Block-V Receiver

| | |
|-------------------------|--------------------------------------------------------------------------------------------------------------------------------------------------|
| Data Formats: | NRZ (-L, -M, -N), Bi- ϕ (-L, -M, -N) |
| Modulation Types: | $\begin{cases} \text{residual - carrier BPSK} \\ \text{suppressed - carrier BPSK} \end{cases}$ |
| Subcarriers: | squarewave, sinewave |
| Symbol Rates: | see Table 2 |
| Carrier Loop Bandwidth: | $B_L \leq \begin{cases} 200 \text{ Hz,} & \text{residual carrier} \\ \min(200 \text{ Hz, } R_{SYM}/20), & \text{suppressed carrier} \end{cases}$ |
| Loop Types: | 2, 3 |

Table 2: Symbol Rates With the Block-V Receiver

| | |
|--------------------|----------------------------------------------------|
| Residual-Carrier | |
| Subcarrier Present | $4 \text{ sps} \leq R_{SYM} \leq 0.67 f_{subcarr}$ |
| Direct Modulation | |
| NRZ | $4 \text{ sps} \leq R_{SYM} \leq 26 \text{ Msps}$ |
| Bi- ϕ | $4 \text{ sps} \leq R_{SYM} \leq 13 \text{ Msps}$ |
| Suppressed-Carrier | |
| Subcarrier Present | $20 B_L \leq R_{SYM} \leq 0.67 f_{subcarr}$ |
| Direct Modulation | |
| NRZ | $20 B_L \leq R_{SYM} \leq 26 \text{ Msps}$ |
| Bi- ϕ | $20 B_L \leq R_{SYM} \leq 13 \text{ Msps}$ |

2.1.1 **Modulation**

The Block-V Receiver supports both residual-carrier and suppressed-carrier Binary Phase-Shift Keying (BPSK). A suppressed carrier is tracked with a Costas loop.

The Block-V Receiver coherently demodulates telemetry subcarriers, whether squarewave or sinewave. Non-Return to Zero (NRZ) and Bi- ϕ (i.e., Manchester) data formats are supported.

When the incoming carrier has a quadriphase signal structure—such as Quadriphase-Shift Keying (QPSK), Offset QPSK, or unbalanced QPSK—with symbols on

both the in-phase and quadrature components of the carrier, the Block-V Receiver can synchronize to the carrier and coherently demodulate and detect the symbols on both of its components. However, the DSN downlink processing currently does not make a provision for dealing with the ambiguous multiplexing of the in-phase and quadrature components inherent in QPSK demodulation. Thus, in the current system configuration, QPSK and OQPSK are not supported by the DSN.

2.1.2 *Symbol Rate*

When tracking a residual carrier, the smallest symbol rate R_{SYM} that can be used is 4 sps. When tracking a suppressed carrier, there is an additional constraint, involving the loop bandwidth B_L of the Costas loop:

$$\frac{R_{SYM}}{B_L} \geq 20, \quad \text{suppressed carrier} \quad (1)$$

It is recommended that the symbol transition density be greater than or equal to 0.25. (It is 0.5 for truly random data.) When the symbol transition density is less than 0.5, more signal-to-noise ratio will be required in the symbol synchronization loop (see section 2.4.5).

The baseband telemetry bandwidth of the Block-V Receiver is 36 MHz (half-power, i.e., -3 dB). In the absence of subcarrier, the maximum symbol rate that the Block-V Receiver can demodulate and detect is 26 Msps for NRZ data and 13 Msps for Bi- ϕ (Manchester) data. The telemetry processing stages that are downstream from the Block-V Receiver are not able to handle such large symbol rates. It is these latter stages that set an upper limit on symbol rate that can be handled by the telemetry subsystem. Module TLM-10 should be consulted for more information.

If the symbol rate is derived from the same frequency source as the subcarrier frequency (i.e., synchronous), it is recommended that there be at least three subcarrier cycles per data symbol. If the subcarrier and symbol rate are asynchronous, a subcarrier frequency to symbol rate ratio of greater than 1.5 is recommended. Furthermore, it is recommended that all proposed combinations of subcarrier frequency and symbol rate be tested to ensure efficient subcarrier demodulation. If the subcarrier and symbol rate are asynchronous, the frequency difference between the subcarrier and any of the first ten harmonics of the symbol rate should be greater than the bandwidth of the subcarrier loop.

2.1.3 *Carrier Loop Bandwidth*

In this module, carrier loop bandwidth means the one-sided, noise-equivalent carrier loop bandwidth of the Block-V Receiver. It will be denoted B_L . The carrier loop bandwidth of the Block-V Receiver may be precisely selected from a continuum of possible values (over some range that is characterized by an upper and lower

limit). Unlike the Block-III and Block-IV Receivers, the Block-V Receiver does not have a predetection bandpass limiter; thus, its carrier loop bandwidth does not vary with signal level. With the Block-V Receiver, the user may make a precise selection for B_L and that selection will continue to characterize the carrier loop even in the presence of a varying signal level. The user may choose to change B_L during a tracking pass and this can be implemented without losing phase-lock, assuming the change is not too large.

There are limits on the carrier loop bandwidth. B_L can be no larger than 200 Hz. The lower limit on B_L is determined by the phase noise on the downlink. In addition, when operating in the suppressed-carrier mode, B_L is subject to the constraint of inequality (1).

In general, the value selected for B_L should be small in order to maximize the carrier loop signal-to-noise ratio. On the other hand, B_L must be large enough that neither of the following variables becomes too large: the static phase error due to Doppler dynamics, the contribution to carrier loop phase error variance due to phase noise on the downlink. The best B_L to select will depend on circumstances. Often, it will be possible to select a B_L of less than 1 Hz. A larger value for B_L is necessary when there is significant uncertainty in the downlink Doppler dynamics, when the sun-earth-probe angle is small (so that solar coronal phase scintillations are present on the downlink), or when the transmitter (such as an Auxiliary Oscillator) has relatively poor frequency stability.

The user may select either a type 2 or type 3 carrier loop. Both loop types are perfect, meaning that the loop filter implements a true accumulation.

2.2 *Definitions*

A residual carrier is present in each of the following cases: with no subcarrier the modulation index is less than 80° , with a squarewave subcarrier the modulation index is less than 80° , with a sinewave subcarrier the peak modulation index is less than 105.5° . The carrier is suppressed when there is either no subcarrier or a squarewave subcarrier and the modulation index is 90° .

P_T is the total received signal power at the input to the low-noise amplifier. N_0 is the one-sided noise spectral density referenced to the input to the low-noise amplifier; it equals the system noise temperature (referenced to the input to the low-noise amplifier) times the Boltzmann constant, $1.380622 \times 10^{-23} \text{ W}/(\text{Hz} \cdot \text{K})$. In decibel units, the Boltzmann constant is $-228.6 \text{ dBW}/(\text{Hz} \cdot \text{K})$. The ratio P_T/N_0 is a useful parameter.

If a single telemetry channel is present and there is a residual carrier, the carrier power P_C and data power P_D are given by

$$P_C = \begin{cases} P_T \cos^2 \theta, & \text{no subcarrier or squarewave subcarrier} \\ P_T J_0^2(\theta), & \text{sinewave subcarrier} \end{cases} \quad (2)$$

$$P_D = \begin{cases} P_T \sin^2 \theta, & \text{no subcarrier or squarewave subcarrier} \\ P_T 2J_1^2(\theta), & \text{sinewave subcarrier} \end{cases} \quad (3)$$

where θ is the peak modulation index. In the case of a sinewave subcarrier, P_D represents the power only in the fundamental harmonics (the only harmonics that will be recovered). With a suppressed carrier, on the other hand, the total received signal power and the data power are the same.

$$P_D = P_T, \quad \text{suppressed carrier} \quad (4)$$

If two telemetry channels are present or if one telemetry channel and a ranging code are present, more complicated expressions are needed. For example, with two telemetry channels, each of which has a squarewave subcarrier (or one with no subcarrier and one with a squarewave subcarrier), the carrier and data powers are:

$$P_C = P_T \cos^2 \theta_1 \cos^2 \theta_2 \quad (5)$$

$$P_{D1} = P_T \sin^2 \theta_1 \cos^2 \theta_2 \quad (6)$$

$$P_{D2} = P_T \cos^2 \theta_1 \sin^2 \theta_2 \quad (7)$$

where P_{D1} and P_{D2} are the data powers for the first and second telemetry channels and θ_1 and θ_2 are the corresponding modulation indices.

The input energy per bit to noise spectral density ratio (bit SNR) is

$$\frac{E_b}{N_0} = \frac{P_D}{N_0 R_{BIT}} \quad (8)$$

where R_{BIT} is the bit rate (before encoding). The energy per symbol to noise spectral density ratio (symbol SNR) is

$$\frac{E_s}{N_0} = \frac{P_D}{N_0 R_{SYM}} \quad (9)$$

where R_{SYM} is the symbol rate (after encoding). For a convolutional code with code rate r ($r = 1/2, 1/4, \text{ or } 1/6$),

$$R_{SYM} = \frac{R_{BIT}}{r} \quad (10)$$

2.3 *Receiver Acquisition*

This section describes normal acquisition of the Block-V Receiver. There is a "Fast Acquisition" algorithm under development for use with the Block-V Receiver, but it is not described here because it is not yet operational and because it is not applicable to all users. (Fast Acquisition can only be used when the symbol rate is low.) No complete description of normal acquisition for the Block-V Receiver has, as yet, been published. Fast Acquisition, which is similar in many respects to normal acquisition of the Block-V Receiver, has been described in Reference 3.

The general procedure for normal acquisition of the Block-V Receiver is as follows. The carrier frequency is measured by searching the downlink signal spectrum in fixed bandwidth sections using a Fast Fourier Transform (FFT). This is as true for suppressed-carrier downlinks as it is for residual-carrier downlinks. With a suppressed carrier, some signal processing that precedes the FFT causes a collapse of data modulation sidebands into a tone (located at the frequency of the phantom carrier) that can be identified by the FFT. Once a tone is found, FFTs are computed for the adjacent bandwidth sections in order to verify that the true tone was found, as opposed to an alias from one of these adjacent bandwidth sections. Then a confirmation FFT, centered at the detected tone, is computed in order to verify that the tone was not a strong signal that was just passing through. Such a set of FFTs produces an accurate measure of the carrier frequency. The Block-V Receiver is designed to also compute, when necessary, a set of FFTs in order to get accurate measures of the subcarrier frequency and symbol rate. Commonly, however, it is not necessary to measure the subcarrier frequency and symbol rate, since their predicts are usually quite accurate. Next, the Numerically-Controlled Oscillator (NCO) in the carrier loop is set with the aid of the information from the FFTs, and the carrier loop is closed (enabled). In the subcarrier loop and symbol loop, the NCOs are set and the loops closed (enabled). The loop closures may be selected to occur in parallel or in series. When the loops are initially closed, the loop gain normalizations are set in accord with available predictions; but when phase-lock is indicated by the lock detectors, the coherent AGCs are enabled, allowing loop gain normalizations to be based on the actual received signal.

2.3.1 *FFT*

The FFT is an optional part of the acquisition process. It is only needed when the signal's frequency uncertainty is greater than one-half the initial loop bandwidth of the tracking loop. Often, only the carrier loop requires the computation of FFTs: the subcarrier and symbol frequencies are often well enough known that they need not be measured with FFTs.

An FFT takes a sequence of data points as input. The sample frequency of these data points, here denoted f_s , depends in general on the type of data being processed and the symbol rate. For the current software delivery (OP-B) of the Block-V Receiver, f_s is given in Table 3.

Table 3: FFT Sample Frequencies

| <u>Data Type</u> | <u>Sample Frequency</u> |
|--------------------|----------------------------------|
| Residual Carrier | 2000 Hz |
| Suppressed Carrier | minimum of 2000 Hz and R_{SYM} |
| Subcarrier | minimum of 500 Hz and R_{SYM} |
| Symbol | minimum of 500 Hz and R_{SYM} |

R_{SYM} is the symbol rate. For the residual-carrier FFT, f_s is 2000 Hz, regardless of the symbol rate. For the suppressed-carrier FFT, f_s equals R_{SYM} when this is less than 2000 Hz; otherwise, f_s is limited to the carrier interrupt rate of 2000 Hz. For the subcarrier and symbol FFTs, f_s equals R_{SYM} when this is less than 500 Hz; otherwise, f_s is limited to 500 Hz.

In general, a number of FFTs may need to be computed before the signal is found. The search bandwidth is explored in sections, with one FFT computed for each section. A section is selected by an appropriate setting of the NCO. This setting determines the center of the section. The bandwidth of each section is determined by the data type and by f_s , as shown in Table 4.

Table 4: FFT Section Bandwidths

| <u>Data Type</u> | <u>Section Bandwidth</u> |
|--------------------|------------------------------------|
| Residual Carrier | $f_s/2: -f_s/2 \rightarrow +f_s/2$ |
| Suppressed Carrier | $f_s/2: -f_s/4 \rightarrow +f_s/4$ |
| Subcarrier | $f_s/2: -f_s/4 \rightarrow +f_s/4$ |
| Symbol | $f_s/2: -f_s/4 \rightarrow +f_s/4$ |

The tone representing the carrier (or subcarrier or symbol rate) will be considered detected within a given section when the corresponding FFT indicates the presence of a tone whose power level falls within an acceptance range centered on the predicted tone power. The acceptance range is characterized by a lower limit delta, δ_{lower} , in decibels and an upper limit delta, δ_{upper} , in decibels. The user of the Block-V Receiver will select the two parameters δ_{lower} and δ_{upper} .

Even after a tone is initially detected, more FFTs will, in general, be computed. An FFT for each of two adjacent sections is computed in order to check for aliases. Such an alias check is, however, optional; if the frequency predictions are quite good, the alias checks are unnecessary.

There is also a confirmation check. This consists of one FFT that is computed with the NCO set to the tone value detected in the previous FFTs. It is used to

verify that the detected tone was not a noise spur (for weak signal acquisitions) and that the tone was not a very strong signal that was simply passing through.

The number of data points that should be selected for input to a particular FFT computation will depend on the predicted tone power. The algorithm that should be used in determining the number of data points is summarized here.

$$\text{Number of Data Points} = 2^M \quad (11)$$

M , the base 2 logarithm of the number of data points, is given by

$$M = \max \left\{ 9, \left\lceil 4.817 - 3.581 \cdot \log_{10} \left(\frac{P_{CTP}}{N_0} \cdot \frac{1}{f_s} \right) \right\rceil \right\} \quad (12)$$

where $\log_{10}(\cdot)$ is the base 10 logarithm and $\lceil \cdot \rceil$ is the ceiling function. The ceiling function equals the smallest integer not less than its argument. The smallest permissible value for M is 9, corresponding to 2^9 data points. P_{CTP}/N_0 is the computed tone power to noise spectral density ratio (as calculated with equation (13) for residual-carrier FFT or with equation (14) for all other FFTs, see below). Figures 2 and 3 illustrate the dependence of the integer M on P_{CTP}/N_0 for $f_s = 2000$ Hz and $f_s = 20$ Hz, respectively.

For the FFT that measures the carrier frequency of a residual-carrier downlink, P_{CTP}/N_0 is given by

$$\frac{P_{CTP}}{N_0} = \left(10^{\delta_{lower}/10} \right) \cdot \frac{P_C}{N_0} \cdot \text{sinc}^2 \left(\frac{1}{2F_{ZP}} \right), \quad \text{residual carrier FFT} \quad (13)$$

where δ_{lower} is a (negative) number representing the delta, in decibels, between the lower limit on acceptance and the predicted tone power level. P_C/N_0 is the residual carrier power to noise spectral density ratio. The $\text{sinc}(\cdot)$ function is: $\text{sinc}(x) = \sin(\pi x)/(\pi x)$. F_{ZP} is the zero pad factor. When $F_{ZP} = 1$, there is no zero padding in the FFT. When $F_{ZP} = 2$, there are as many zeros padded to the end of the data points as there are data points. The size of the sequence that is input to the FFT equals F_{ZP} times the number of data points.

For all other FFTs (i.e., for all FFTs except that for the carrier frequency of a residual-carrier downlink), P_{CTP}/N_0 is given by

$$\frac{P_{CTP}}{N_0} = \left(10^{\delta_{lower}/10} \right) \cdot \frac{R_{SYM}(E_S/N_0)}{\alpha_1 + \alpha_2(E_S/N_0)^{-1}} \cdot \text{sinc}^2 \left(\frac{1}{2F_{ZP}} \right), \quad \text{all other FFTs} \quad (14)$$

Figure 2: Number of Data Points for FFT; Sample Rate = 2000 Hz

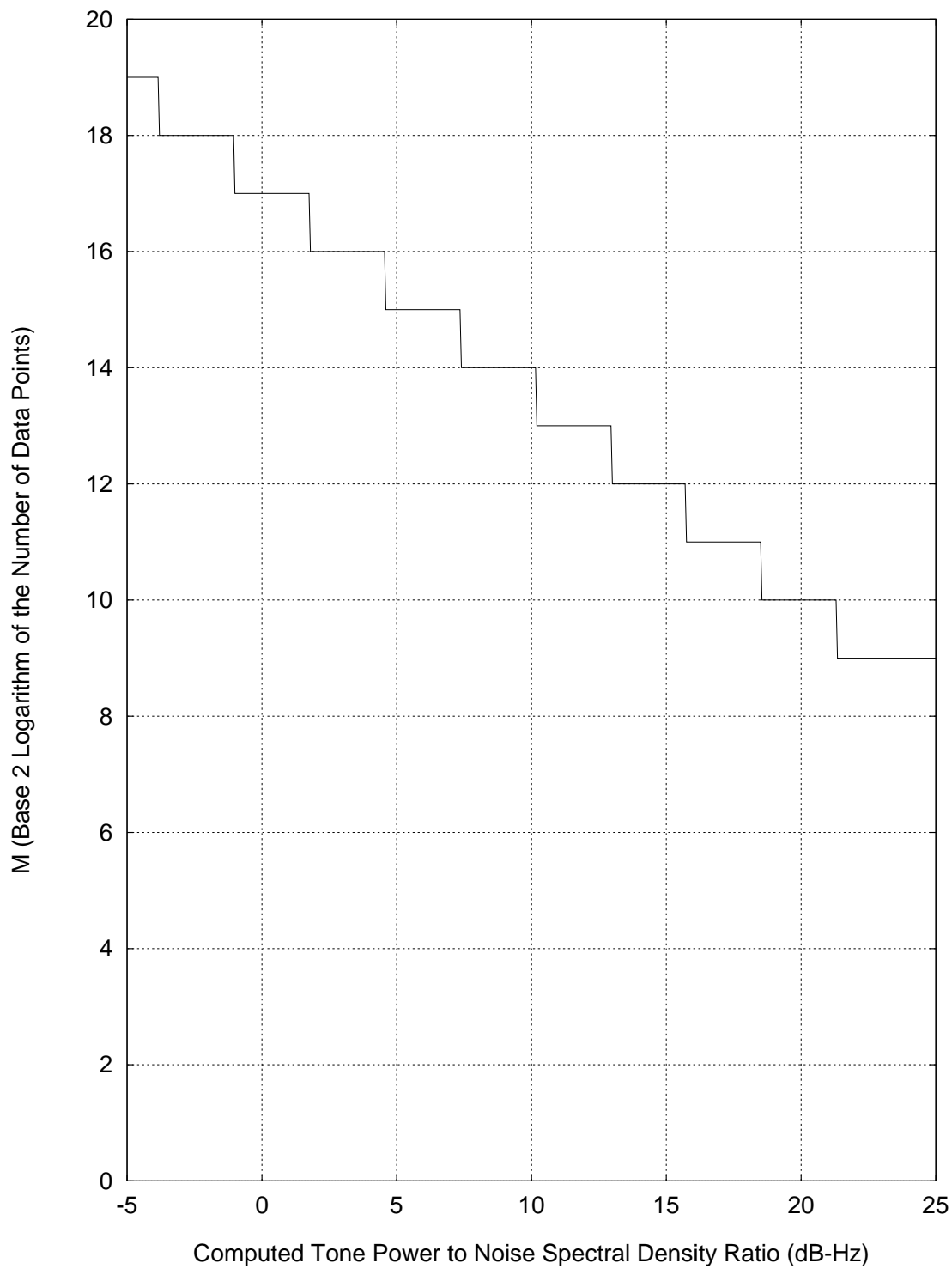
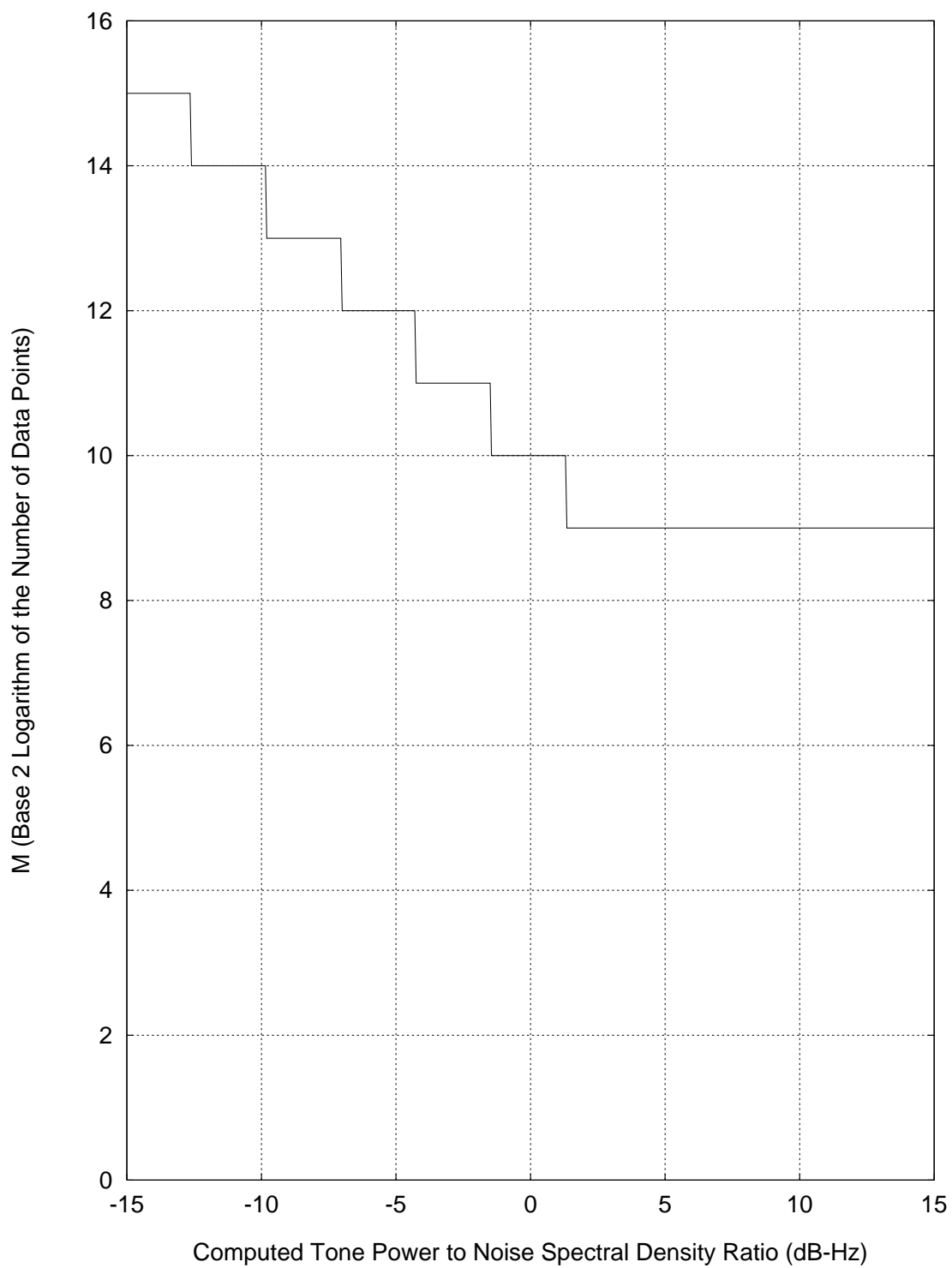


Figure 3: Number of Data Points for FFT; Sample Rate = 20 Hz



R_{SYM} is the symbol rate, and E_s/N_0 is the predicted energy per symbol to noise spectral density ratio. The coefficients α_1 and α_2 depend on the particular FFT. Table 5 lists these values. For example, for an FFT that is computed in order to identify the symbol rate, the coefficients α_1 and α_2 are 390 and 880, respectively, when there is a squarewave subcarrier present. For all loops besides the residual carrier loop, the data modulation sidebands are employed. That is the reason equation (14) is more complicated than equation (13). Equation (14) is valid under the assumption that all loops are slipping (i.e., that none of the loops have acquired phase-lock) as the data points are being collected. If some loops have acquired phase-lock before the data points are collected for subsequent FFTs, then the P_{CTP}/N_0 given in equation (14) will be somewhat pessimistic for these subsequent FFTs. Equations (13) and (14) are based on modifications to the theory presented in Reference 3. (The modifications are necessary since the theory of Reference 3 is for the Fast Acquisition algorithm, which is not described in this module.)

Table 5: Coefficients α_1 and α_2 in the Calculation of P_{CTP}/N_0

| FFT | Subcarrier | α_1 | α_2 |
|--------------------|------------|------------|------------|
| ----- | ----- | ----- | ----- |
| Suppressed Carrier | none | 6 | 4.5 |
| Suppressed Carrier | square | 18 | 41 |
| Subcarrier | square | 18 | 41 |
| Subcarrier | sine | 12 | 18 |
| Symbol | none | 130 | 100 |
| Symbol | square | 390 | 880 |
| Symbol | sine | 260 | 390 |

2.3.2 *Loop Locking*

Once the carrier frequency has been found, the NCO in the carrier loop is set to the detected frequency and the carrier loop is closed (enabled). The loop starts at an initial bandwidth. The loop phase error, initially large, diminishes with time through the natural feedback action of the loop. Once phase-lock is declared at this bandwidth, the loop bandwidth is gradually reduced to its final value -- the desired operational value -- in a manner consistent with the retention of phase-lock. When the final bandwidth has been achieved and the degradation to effective signal level resulting from transient phase errors just drops below 0.1 dB, the receiver is considered to be acquired. The initial and final bandwidths are controlled by the user, along with the parameters that control the rate at which the bandwidth is narrowed. Starting with loop closure, the time it takes for the lock detector to indicate phase-lock at the final bandwidth is approximately ten times the reciprocal of the final bandwidth. (For purposes of estimating acquisition time, however, it is recommended that twenty times the reciprocal of the final loop bandwidth be used. This admits of the possibility that phase-lock is not indicated in the first lock detection period.) The final step in the procedure is for the coherent AGC loop to be enabled, providing an accurate estimate of the loop normalization constant.

The locking of the subcarrier and symbol loops is a similar process to that described in the previous paragraph for the carrier loop. The subcarrier and symbol loops may either be closed (enabled) at the same time that the carrier loop is closed (enabled) or be closed after the carrier loop has indicated phase-lock. It is the user's choice. In the former case, all three loops are simultaneously trying to achieve phase-lock. For the (squarewave) subcarrier and symbol loops, there is also a transition window, which has an initial value, a final value, and a parameter that controls the rate of narrowing.

2.3.3 *Acquisition Time*

The total acquisition time for the Block-V Receiver is estimated as a sum of two components: the time required for the FFT stage of the acquisition process and the time required for locking the loops.

There is a time associated with the collection of enough data points as required for each FFT. For a given FFT, this time equals the number of data points divided by the sample frequency.

$$\text{Time for each FFT} = \frac{2^M}{f_s} \quad (15)$$

where M is given by equation (12). The time required to actually compute an FFT is often small compared with the time it takes to collect the data points for input to that FFT. (The time it takes to pad an input sequence with zeros is also small.) Hence, it is often a good approximation to use equation (15) to estimate the time it takes to produce one FFT.

It is necessary to consider how many FFTs might be required and to sum together the individual FFT times in order to estimate the time spent on the FFT stage of the acquisition process. Consideration must be given to whether subcarrier or symbol FFTs will be required. Often, it is not necessary to compute FFTs in support of subcarrier and symbol acquisition. In the best possible scenario, in which carrier frequency, subcarrier frequency and symbol rate are all very accurately characterized by their predicts, no FFTs are required. In a more typical scenario, however, at least two FFTs will be required for the carrier: an initial FFT and a confirmation FFT. In some cases, more FFTs will be required for carrier acquisition: the search bandwidth may be larger than a single section bandwidth and alias checking may be required.

A second component of receiver acquisition time is the time required for the loops to lock once their NCOs have been set. For each loop, phase-lock will be achieved and duly indicated by the lock detector in a time that may be estimated as

$$\text{Time for each loop} = \frac{20}{B} \quad (16)$$

B represents the final loop bandwidth of the loop in question (carrier, subcarrier, or symbol). The numerator in this estimate is twenty, rather than ten, allowing for the possibility that phase-lock is not indicated in the first lock detection period. Figure 4 illustrates this dependence. If the loops are acquired in parallel, the loop-locking component of receiver acquisition time may be estimated from equation (16) with the smallest of all loop bandwidths substituted for B . Typically, the smallest loop bandwidth is that of the symbol loop. If the loops are acquired in series, the loop-locking component of receiver acquisition time may be estimated as the sum of the individual loop-locking times, each of which may be estimated from equation (16) with the substitution of the appropriate loop bandwidth. In general, the following factors will influence the user's choice of loop bandwidths: P_T/N_0 , doppler dynamics, oscillator stability, and acquisition time. For example, larger values of P_T/N_0 will permit larger loop bandwidths (for more details, see section 2.4).

For many applications the receiver acquisition time will be one minute or less. However, when the symbol rate and the symbol loop bandwidth are small, the acquisition time can be much larger, as large as twenty minutes in extreme cases. The discussion and equations of this section will serve as a guide to estimating the receiver acquisition time.

It would be very difficult to provide here a set of curves characterizing receiver acquisition time for all potential cases of interest. There are just too many possibilities. Not only are there a number of important variables (symbol rate, signal-to-noise ratio, loop bandwidths, quality of frequency predictions) with large dynamic ranges, but the flexibility of the Block-V Receiver permits a wealth of different acquisition strategies. Alias-check FFTs and confirmation-check FFTs may or may not be used. Subcarrier FFTs and symbol rate FFTs may or may not be used. The loops may be acquired in parallel, in series, or in some other combination. (For example, the carrier loop might be acquired first, then the subcarrier and symbol loops might be acquired in parallel.) Although it is not practical to provide curves for all potential cases of interest, three sets of curves are provided in order to illustrate how receiver acquisition time varies with certain key parameters.

Figures 5, 6, and 7 show receiver acquisition time for a very specific set of assumptions. For all three of these figures, the frequency predicts are good enough that only two carrier FFTs (an initial FFT and a confirmation-check FFT) are necessary and that no subcarrier or symbol rate FFT is required. Furthermore, it is assumed that the loops are acquired in parallel. For these figures the receiver acquisition time is calculated as twice the "Time for each FFT", as given by equation (15), plus $20/B$, where B is the smallest loop bandwidth (typically the symbol loop bandwidth). The integer M in equation (15) is calculated from equations (12) and (13) or (14). F_{zp} taken to be 1 (i.e., no zero padding) and δ_{lower} taken to be -2 dB.

Figure 4: Loop Locking Time

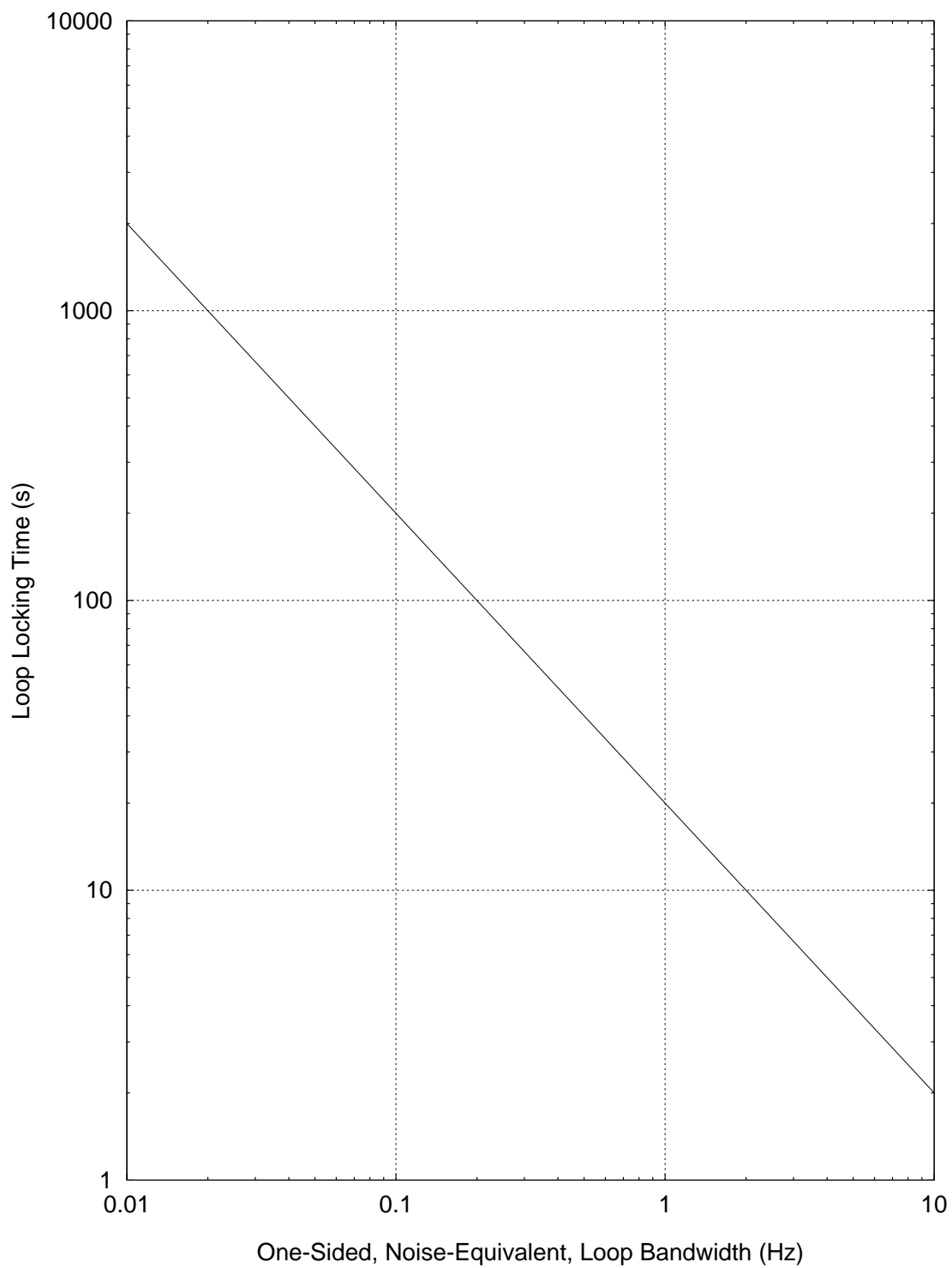


Figure 5: Receiver Acquisition Time; Residual Carrier

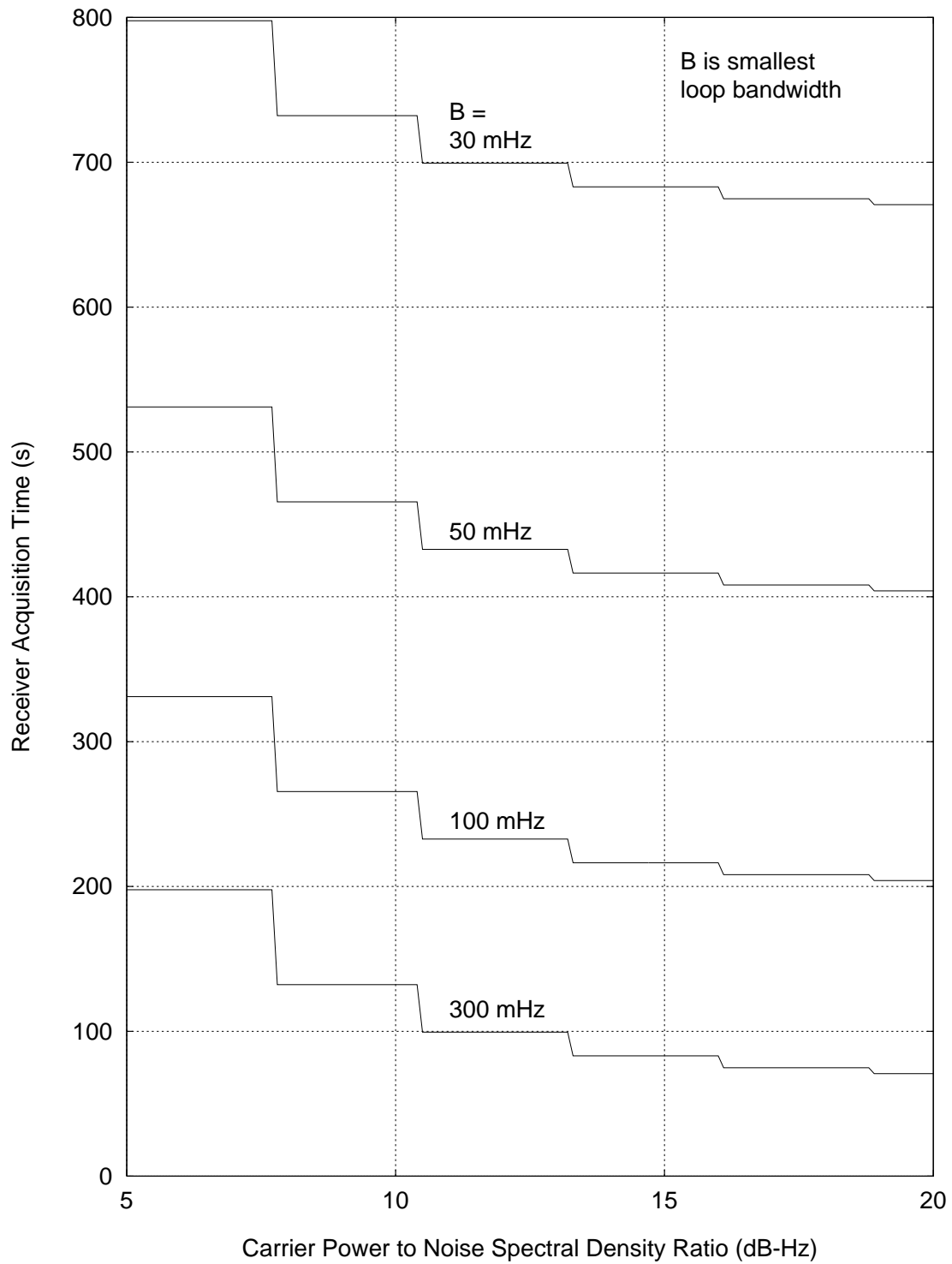


Figure 6: Receiver Acquisition Time; Suppressed Carrier

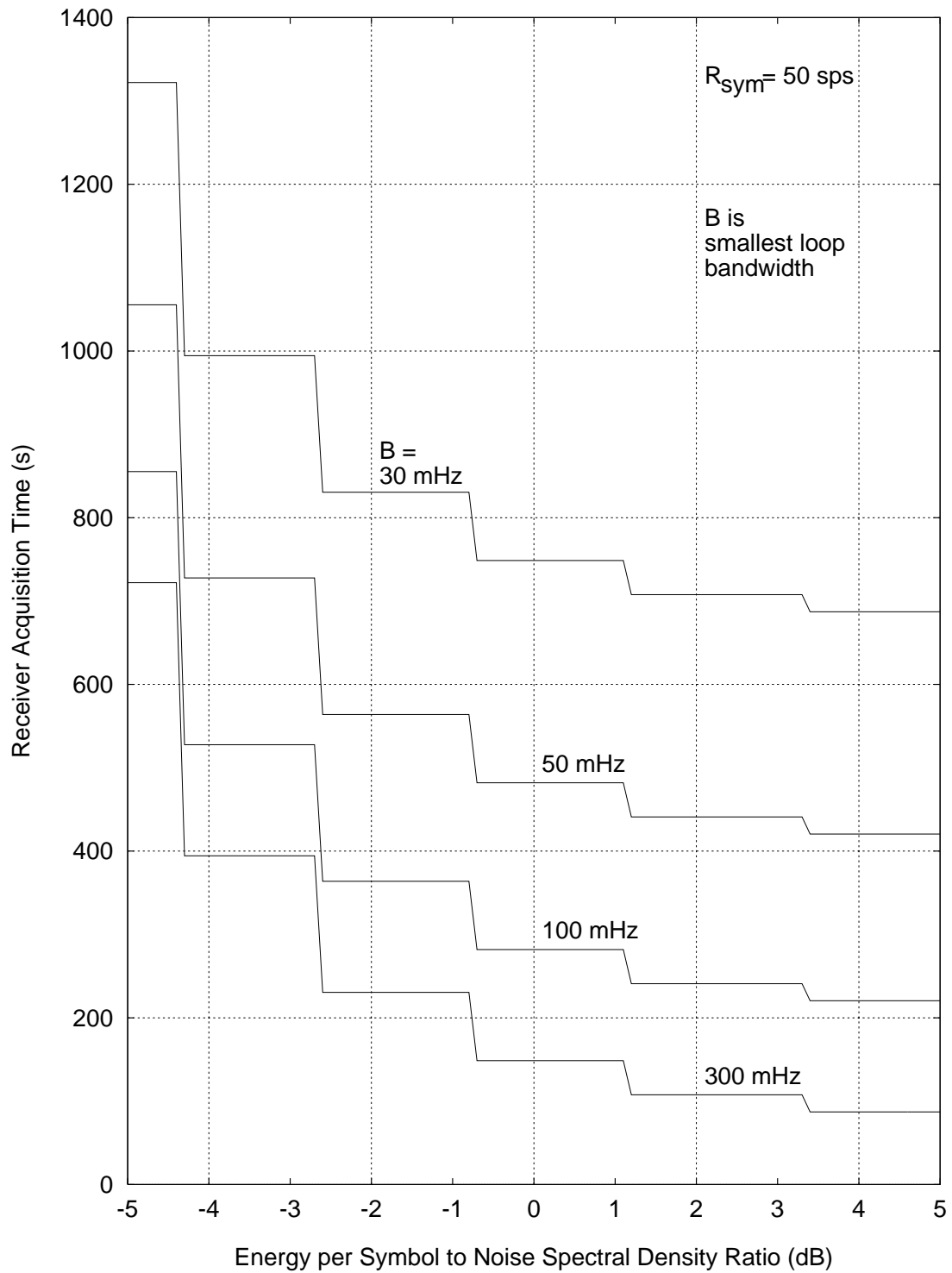


Figure 7: Receiver Acquisition Time; Suppressed Carrier

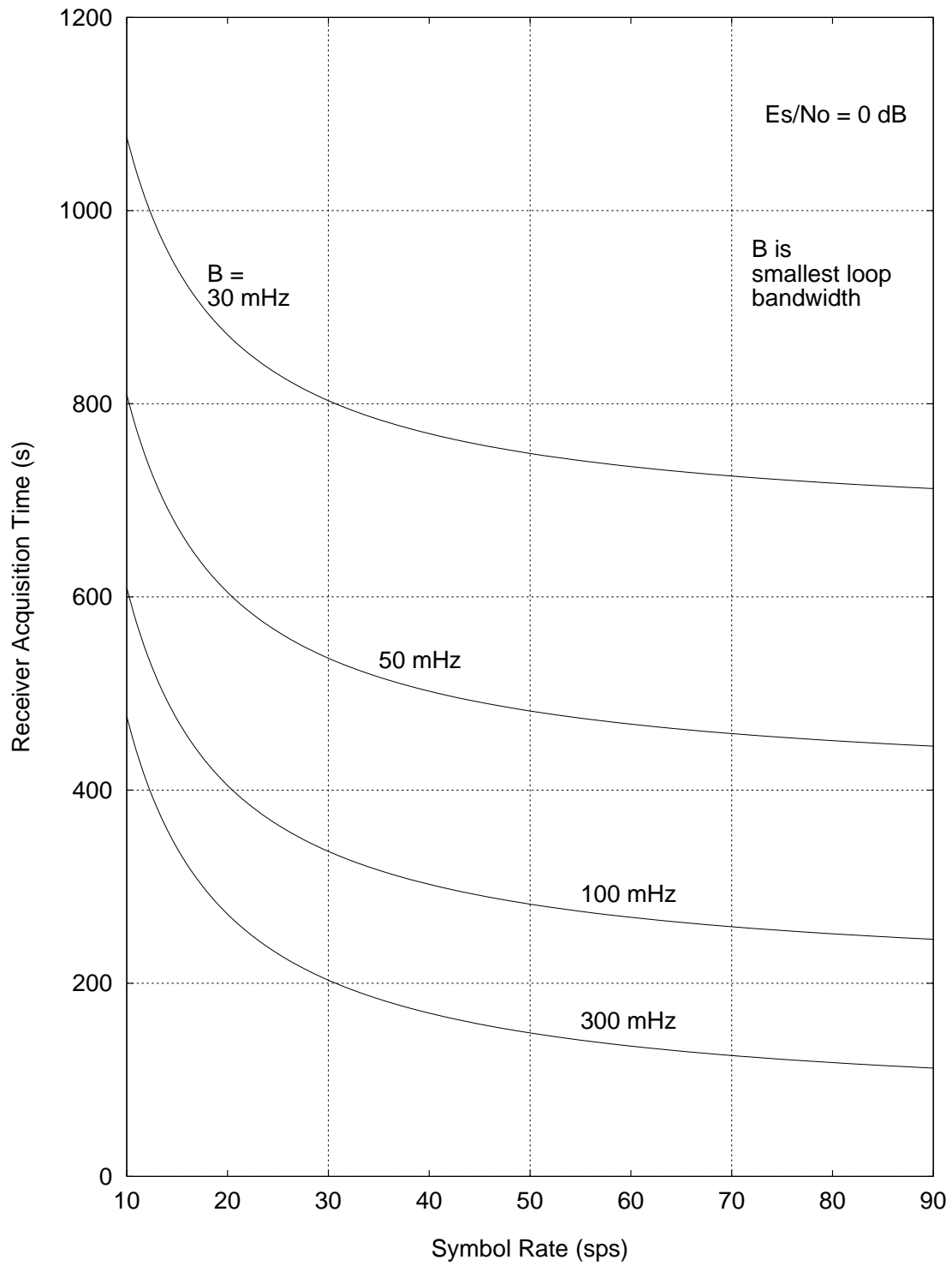


Figure 5 shows the receiver acquisition time (in seconds) for a residual-carrier downlink as a function of P_C/N_0 with B , the smallest loop bandwidth, as a parameter. The frequency predicts have to be reasonably good to achieve the acquisition times shown in this figure: the carrier must lie within the section bandwidth of the first FFT and the subcarrier frequency and symbol rate must be well enough known to obviate the need for their measurement.

Figure 6 shows the receiver acquisition time (in seconds) for a suppressed-carrier downlink as a function of E_s/N_0 with B , the smallest loop bandwidth, as a parameter. The symbol rate R_{SYM} is 50 sps. The frequency predicts have to be reasonably good to achieve the acquisition times shown in this figure: the collapsed carrier tone must lie within the section bandwidth of the first FFT and the subcarrier frequency and symbol rate must be well enough known to obviate the need for their measurement.

Figure 7 shows the receiver acquisition time (in seconds) for a suppressed-carrier downlink as a function of R_{SYM} with B , the smallest loop bandwidth, as a parameter. The energy per symbol to noise spectral density ratio is 0 dB. The frequency predicts have to be reasonably good to achieve the acquisition times shown in this figure: the collapsed carrier tone must lie within the section bandwidth of the first FFT and the subcarrier frequency and symbol rate must be well enough known to obviate the need for their measurement.

The standard deviation of receiver acquisition time should be approximated as 50% of the expected acquisition time as given in Figures 5, 6, and 7 or as calculated using equations (15) and (16).

A comparison of Figures 5, 6, and 7 reveals that the receiver acquisition time increases as the symbol rate decreases, the signal-to-noise ratio decreases, or the loop bandwidths decrease. Also, the receiver acquisition time for suppressed-carrier operation will generally be larger than for residual-carrier operation.

2.4 *Telemetry Performance*

In general, four signal-to-noise ratios affect telemetry performance: the energy per bit to noise spectral density ratio and the signal-to-noise ratios in each of the three synchronization loops (carrier, subcarrier, and symbol). In some cases (especially with a suppressed carrier) there will be no subcarrier present. In order for telemetry to be supported at a given bit rate, P_T/N_0 must be large enough that these four (or three, if there is no subcarrier) signal-to-noise ratios are adequate. The paragraphs of this section offer guidance in this matter.

2.4.1 *Comparison of Residual Carrier and Suppressed Carrier*

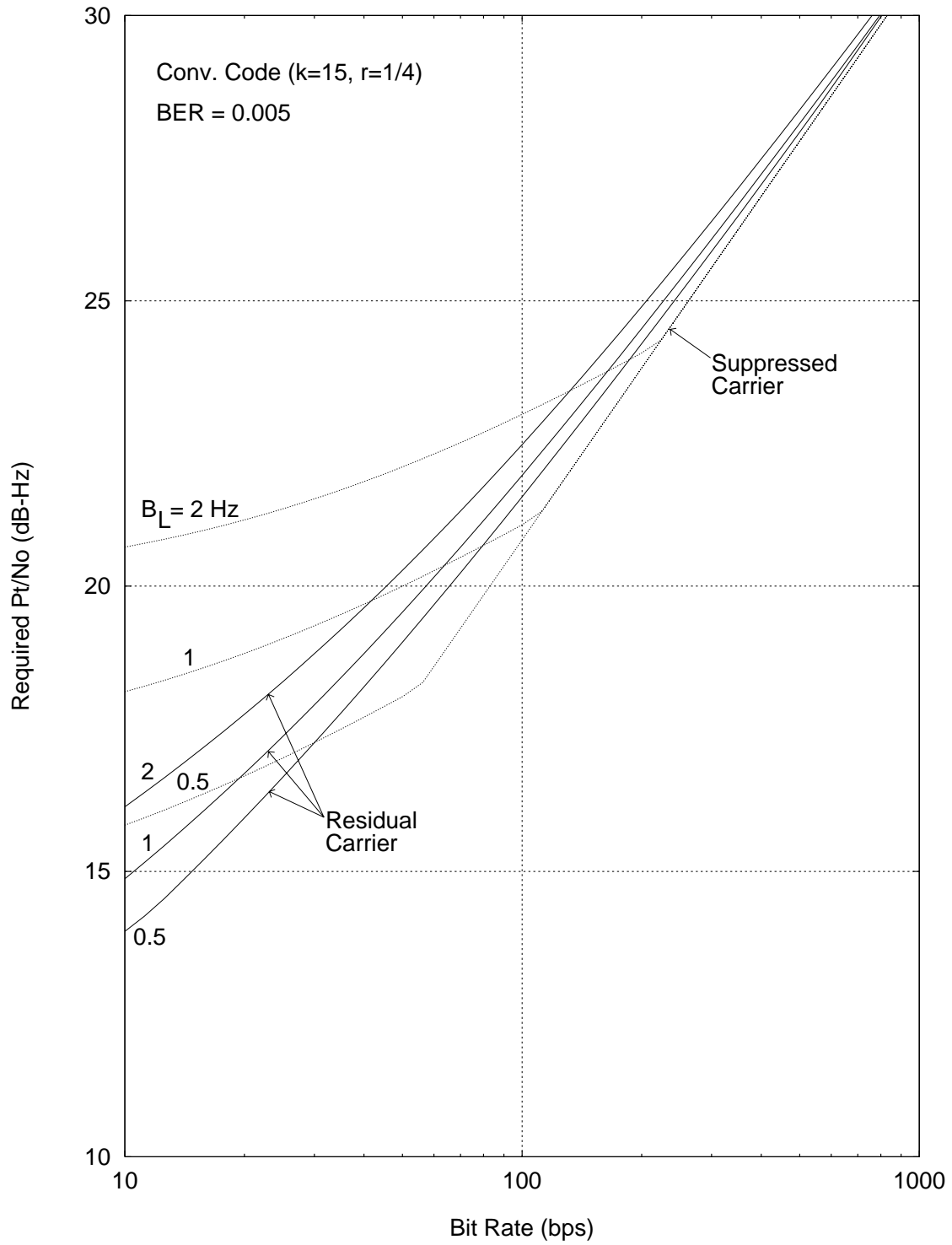
The relative telemetry performance of residual-carrier operation and suppressed-carrier operation depends strongly on the bit rate. One scheme is said to have better telemetry performance than the other when it has a smaller required P_T/N_0 for the support of a given bit rate at a given threshold BER. In general, residual carrier has the better telemetry performance for the very low bit rates and especially for low bit rates coupled with larger carrier loop bandwidths (as would be necessary in the presence of significant phase noise or uncompensated Doppler dynamics). For intermediate bit rates, suppressed carrier offers a significant telemetry performance advantage over residual carrier. For high bit rates, suppressed carrier offers a telemetry performance advantage, but it is only about 0.1 dB. Of course, there will be times in which the decision between residual carrier and suppressed carrier is made on grounds having nothing to do with telemetry performance. For example, a residual carrier is sometimes needed for a radio science experiment.

Figure 8 shows a typical case. It compares the required P_T/N_0 as a function of bit rate R_{BIT} for residual-carrier and suppressed-carrier operation in the case where a convolutional ($k=15, r=1/4$) code is employed and the threshold BER is 5×10^{-3} . Three carrier loop bandwidths are considered: 0.5 Hz, 1 Hz, and 2 Hz.

For Figure 8 it has been assumed that there is no additional phase noise present in the carrier loop beyond that resulting from thermal noise. The required P_T/N_0 is, in this case, the minimum P_T/N_0 that simultaneously meets each of the following four constraints. First, the carrier loop signal-to-noise ratio (ρ_L , see section 2.4.3) must be at least 10 dB if tracking a residual carrier or at least 17 dB if tracking a suppressed carrier. Second, the squarewave subcarrier loop signal-to-noise ratio (ρ_{SUB} , see section 2.4.4) must be at least 20 dB. Third, the symbol loop signal-to-noise ratio (ρ_{SYM} , see section 2.4.5) must be at least 15 dB. Fourth, the product $\eta_{SYS} \cdot E_b/N_0$ must be at least 0.5 dB. System loss η_{SYS} is here calculated using the medium-rate model for radio loss (see Appendix B). For each residual-carrier performance curve it is assumed that at each point on the curve the optimum modulation index is used. The subcarrier loop bandwidth and window factor are assumed to be 50 mHz and 0.25, respectively. The symbol loop bandwidth and window factor are assumed to be 50 mHz and 0.25, respectively.

For the case represented in Figure 8 with $B_L = 0.5$ Hz, residual carrier offers better telemetry performance than suppressed carrier for bit rates less than 30 bps, and suppressed carrier is better for bit rates greater than 30 bps. With $B_L = 1$ Hz, the performances of residual carrier and suppressed carrier cross at 65 bps. With $B_L = 2$ Hz, they cross at 130 bps. These numbers are specific to the example considered here. However, the essential qualitative features of the curves shown in Figure 8 are true in general. Residual carrier is better at low bit rates, and suppressed carrier is better at intermediate bit rates (but there is not much difference at high bit rates). The bit rate for which the two performance curves cross increases with carrier loop bandwidth.

Figure 8: Comparison of Residual Carrier and Suppressed Carrier



The reason residual carrier performs better than suppressed carrier at the low bit rates is because a residual-carrier loop is not subject to half-cycle slips. A suppressed-carrier loop, on the other hand, can slip a half-cycle and therefore requires a higher carrier loop signal-to-noise ratio in order to guard against these damaging slips. (A residual-carrier loop can slip a whole cycle, but this is both less likely and less damaging than a half-cycle slip.)

In order to get the best performance from residual-carrier operation, it is necessary that the modulation index be optimal or, at least, near optimal. Each residual-carrier performance curve of Figure 8 is based on the assumption that the modulation index is optimized at each point on the curve. Figure 9 shows what happens if this is not the case. In Figure 9, the lower curve (with the better telemetry performance) is the same as the residual carrier curve with $B_L = 1$ Hz of Figure 8, with an optimized modulation index at each point on the curve. The upper curve of Figure 9 represents residual-carrier performance with $B_L = 1$ Hz under all the same circumstances except that the modulation index is not optimized at each point on the curve; instead, a single modulation index of 52° (the optimum modulation index for a bit rate of 10 bps) is used for the entire curve. The two curves of Figure 9 coalesce at $R_{BIT} = 10$ bps, of course. But for R_{BIT} greater than 10 bps, a penalty is paid for not using the appropriate optimum modulation index. At $R_{BIT} = 1000$ bps, the penalty is about 2 decibels.

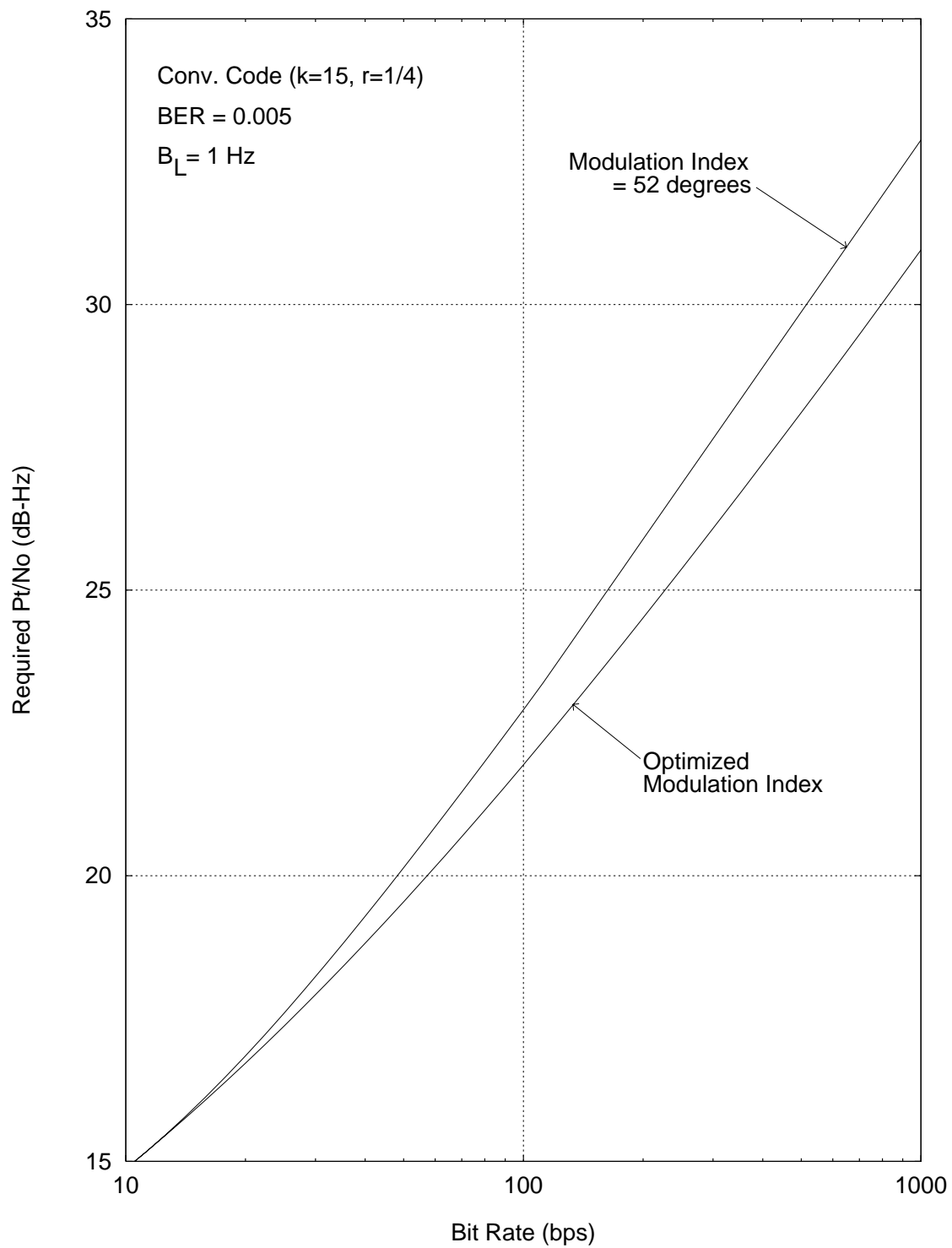
2.4.2 *Decoding Threshold and System Loss*

Telemetry will not be properly decoded unless the product $\eta_{SYS} \cdot E_b/N_0$ is greater than or equal to the effective threshold energy per bit to noise spectral density ratio, $f^{-1}(\text{BER})$, that is required by the coding scheme. η_{SYS} is the system loss, BER is the threshold bit error rate, and $f(\cdot)$ is the ideal functional dependence of probability of bit error on bit SNR (see Appendix A). Table 6 lists the effective threshold energy per bit to noise spectral density ratio, $f^{-1}(\text{BER})$, that is required by an uncoded link and by each of three different convolutionally coded links. For comparable information on a Reed-Solomon code concatenated with a convolutional code, see module TLM-40.

Table 6: Effective Threshold Energy per Bit to Noise Spectral Density Ratio

| Code | 5×10^{-3} | 10^{-3} | 10^{-4} | 10^{-5} |
|-----------------------|--------------------|-----------|-----------|-----------|
| ----- | ----- | ----- | ----- | ----- |
| Uncoded | 5.2 | 6.8 | 8.4 | 9.6 |
| ($k = 7, r = 1/2$) | 2.3 | 3.0 | 3.8 | 4.5 |
| ($k = 15, r = 1/4$) | 0.5 | 0.9 | 1.5 | 2.0 |
| ($k = 15, r = 1/6$) | 0.3 | 0.7 | 1.3 | 1.8 |

Figure 9: Comparison of Optimized and Nonoptimized Modulation Index



The system loss η_{SYS} ($0 < \eta_{SYS} \leq 0.93$) is a composite loss factor used in communication link budgets to account for the following influences on telemetry efficiency: imperfect carrier, subcarrier and symbol synchronization and waveform distortion.

$$\eta_{SYS} = \min\{0.93, \eta_{RADIO} \cdot \eta_{SUB} \cdot \eta_{SYM} \cdot \eta_{WD}\} \quad (17)$$

η_{RADIO} is radio loss, η_{SUB} is subcarrier demodulation loss, η_{SYM} is symbol synchronization loss and η_{WD} is waveform distortion loss. The component losses are estimated separately and the results multiplied (or their decibel equivalents added) to get the composite system loss. If the product of the component losses is not less than 0.93, then η_{SYS} should be estimated as 0.93 (i.e., $-10 \log \eta_{SYS} = 0.3$ dB).

2.4.3 *Carrier Synchronization*

Two different circuits are used for carrier synchronization, depending as the tracking is residual carrier or suppressed carrier. The suppressed carrier circuit is a Costas loop.

2.4.3.1 *Residual Carrier*

A residual carrier signal can be tracked whether or not there is a subcarrier (squarewave or sinewave) present and whether the symbols are non-return-to-zero or Manchester.

When tracking a residual carrier, the carrier loop signal-to-noise ratio is

$$\rho_L = \frac{P_C}{N_0 B_L} \quad (18)$$

There is an additional loss to the carrier loop signal-to-noise ratio when tracking a residual carrier with non-return-to-zero symbols in the absence of a subcarrier. This loss is due to the presence of data sidebands overlaying the residual carrier in the frequency domain and therefore increasing the effective noise level for carrier synchronization. ρ_L , in this case, must be calculated as (Reference 4)

$$\rho_L = \frac{P_C}{N_0 B_L} \cdot \frac{1}{1 + 2 E_s / N_0} \quad (19)$$

Imperfect carrier synchronization results in a higher bit error probability for the recovered telemetry data than would be the case if perfect tracking could be achieved. Radio loss is a measure of this discrepancy between the ideal and what is achieved in practice. Figures 10, 11, 12 and 13 show the effect of radio loss with residual carrier. Figure 10 is for uncoded telemetry. Figures 11, 12 and 13 are for convolutionally coded

($k = 7, r = 1/2$), ($k = 15, r = 1/4$) and ($k = 15, r = 1/6$) telemetry, respectively. For each of these figures it has been assumed that subcarrier and symbol synchronization and waveform symmetry is perfect and that transmitter and solar phase noise is negligible. Furthermore, it has been assumed that the high-rate radio loss model is valid. Hence, for Figures 10 through 13, $\eta_{SYS} = \eta_{RADIO} = \eta_{HRM}$. The high-rate model with residual-carrier tracking and static phase error is defined by equations (B-2) and (B-6) of Appendix B. In equation (B-6) the substitution $\sigma_\phi^2 = 1/\rho_L$ has been made; this is the assumption of negligible transmitter and solar phase noise. The purpose of these four figures is to show the effect of imperfect carrier synchronization (due to thermal noise and static phase error) on telemetry performance.

The radio loss in decibels (i.e., $-10 \log \eta_{RADIO}$) is simply the horizontal distance between the baseline curve and the curve that represents performance in the presence of imperfect carrier synchronization. In comparing several curves from any one figure, it is evident that radio loss is a function of both ρ_L and the threshold BER. In comparing different figures, it is evident that radio loss is a function of the coding scheme.

In each of Figures 10 through 13, there are three curves, corresponding to static phase errors of 0, 3, and 5 degrees, for each value of ρ_L . Uncompensated Doppler dynamics cause static phase error (Appendix C).

With residual-carrier tracking it is important to make an optimal selection of the modulation index. In general, the optimum value for modulation index is a function of the bit rate, the carrier loop bandwidth, the coding scheme, and the threshold BER. Figure 14 shows the optimum modulation index for uncoded telemetry. Figures 15 and 16 show the optimum modulation index for convolutionally coded ($k = 7, r = 1/2$) and ($k = 15, r = 1/4$) telemetry, respectively. The optimum modulation index for convolutionally coded ($k = 15, r = 1/6$) telemetry is approximately the same as that for ($k = 15, r = 1/4$) telemetry.

The curves of Figures 14 through 16 are defined by two constraints: ρ_L should be greater than or equal to 10 dB and the product $\eta_{RADIO} \cdot E_b/N_0$ should be greater than the threshold effective energy per bit to noise spectral density ratio (as given in Table 6) corresponding to a threshold BER of 5×10^{-3} . The medium-rate radio loss model, the most generally applicable model for radio loss, has been used.

To good approximation, the optimum modulation indices of Figure 15 may also be used for a concatenated Reed-Solomon (255, 223) / convolutional ($k = 7, r = 1/2$) code with an end-to-end threshold BER of 10^{-5} .

Figure 10: Telemetry Performance; Uncoded, Residual Carrier

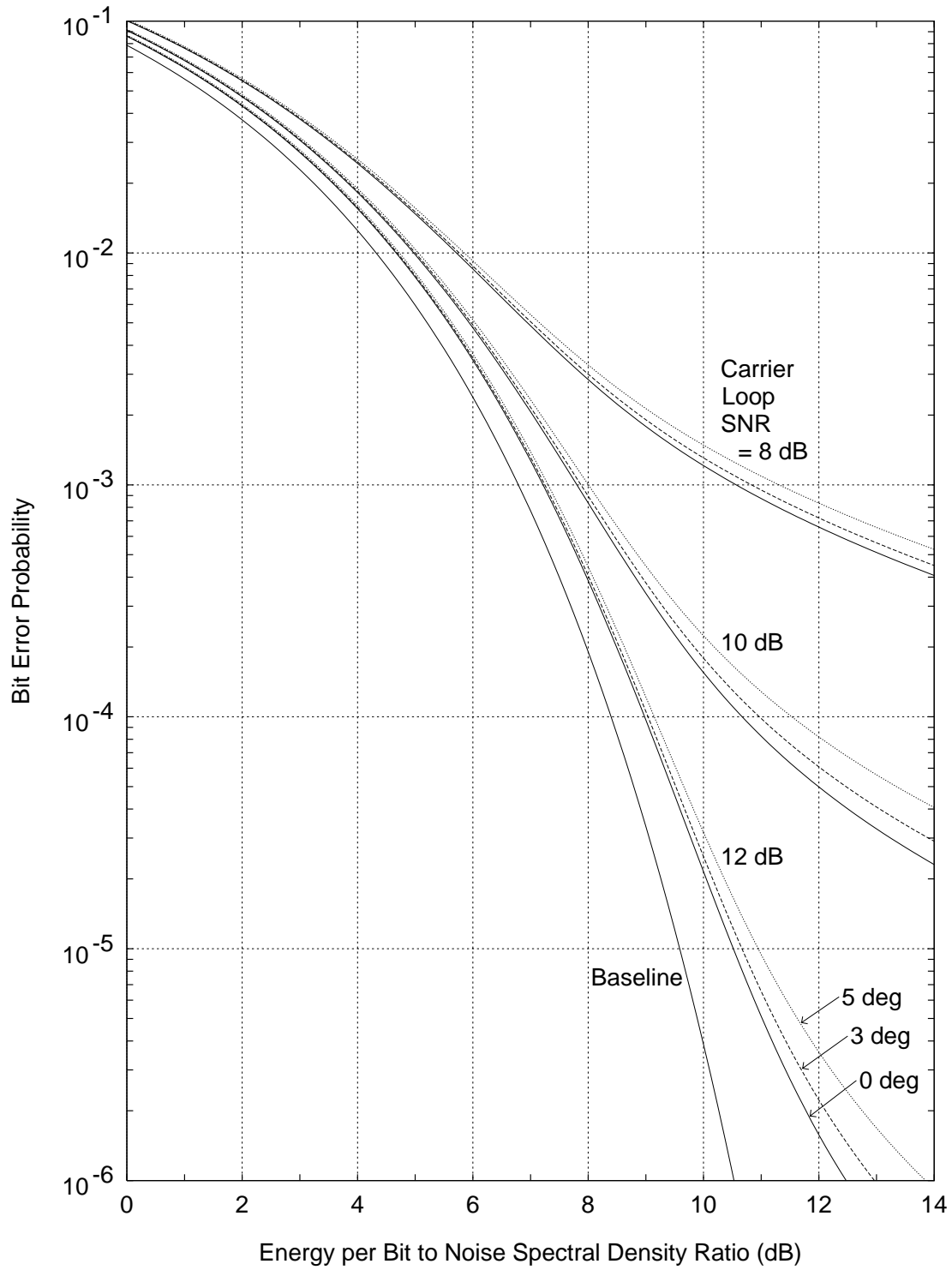


Figure 11: Telemetry Performance; Conv. Code ($k=7$, $r=1/2$), Residual Carrier

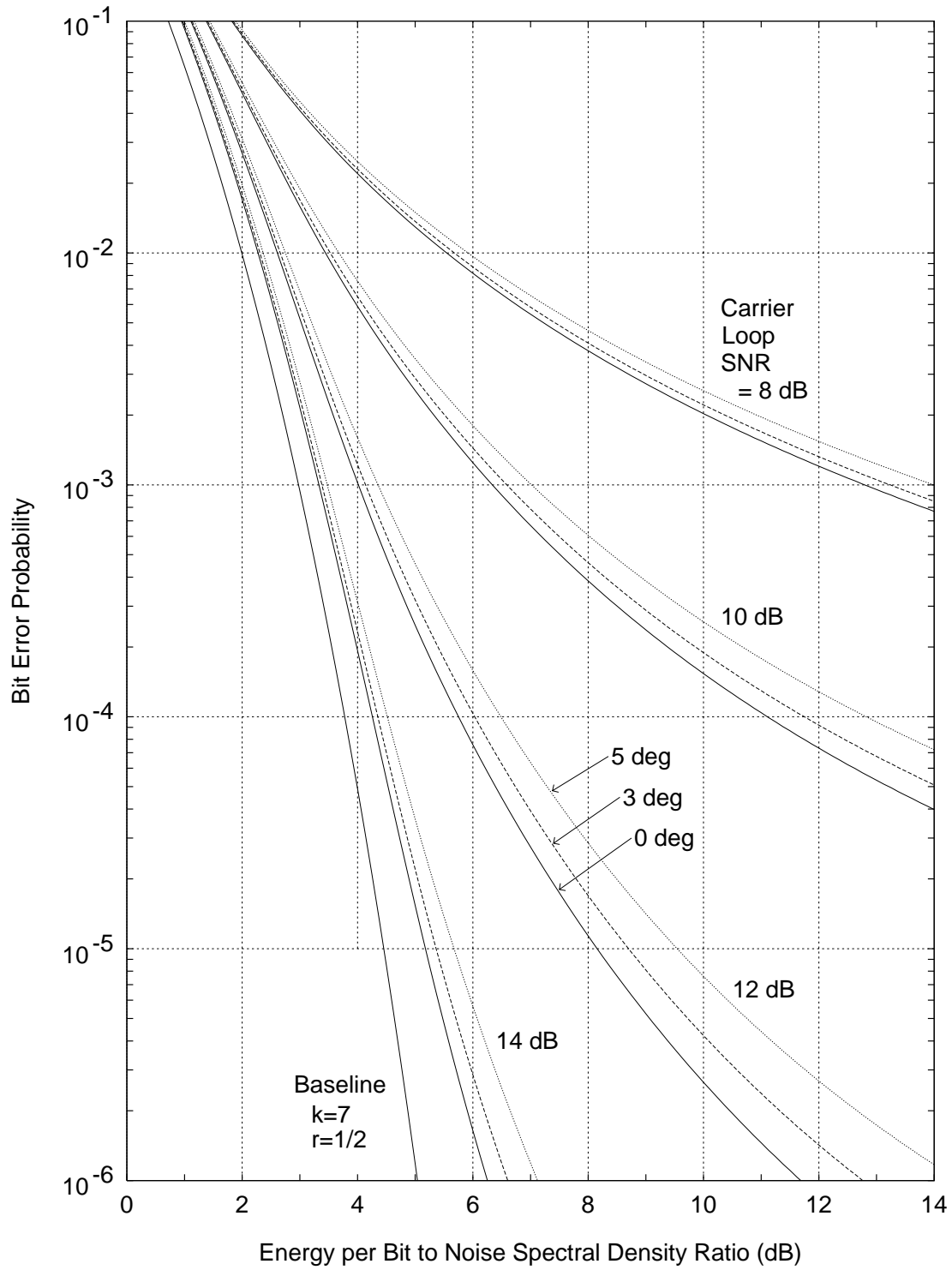


Figure 12: Telemetry Performance; Conv. Code ($k=15$, $r=1/4$), Residual Carrier

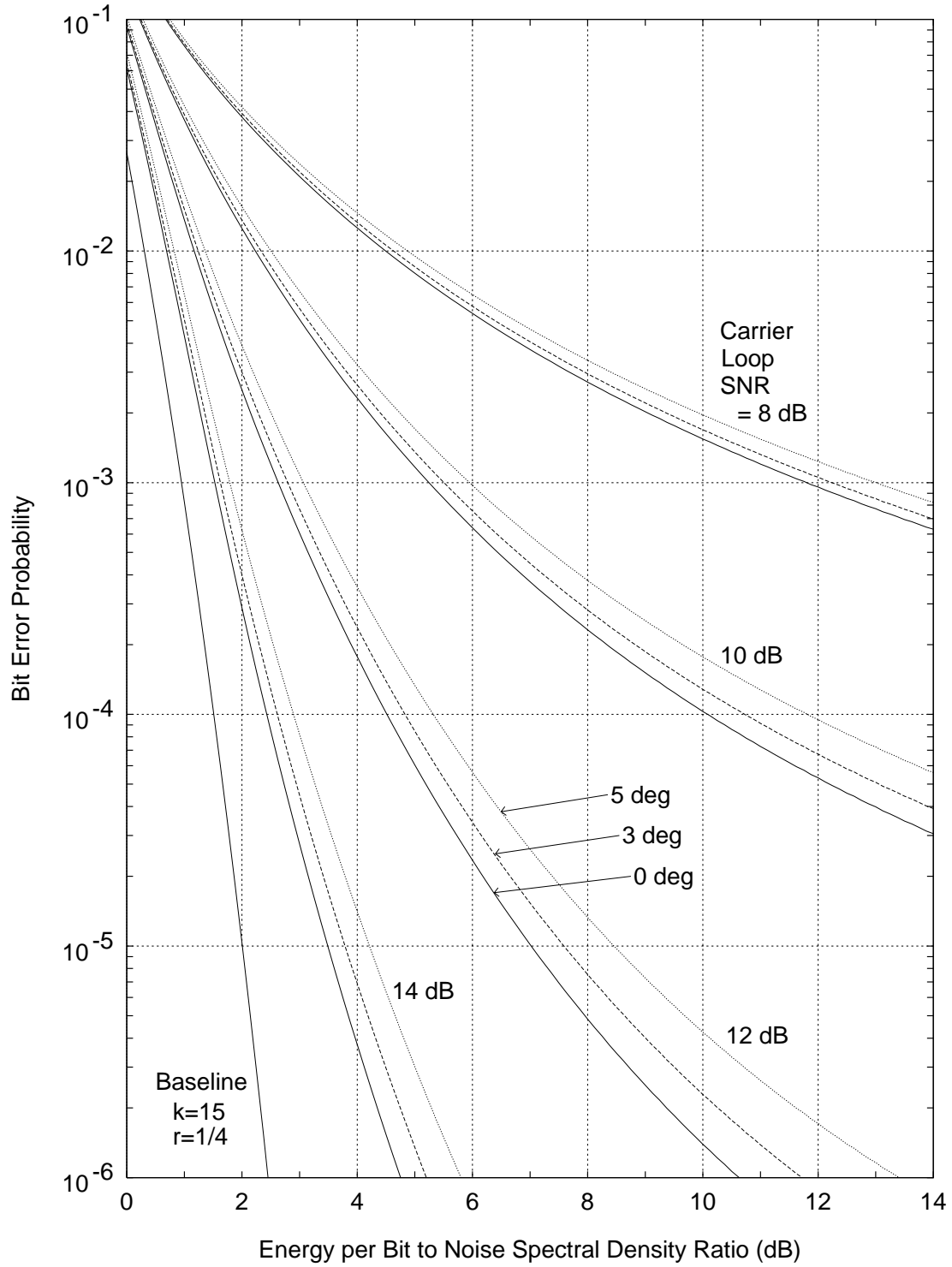


Figure 13: Telemetry Performance; Conv. Code ($k=15$, $r=1/6$), Residual Carrier

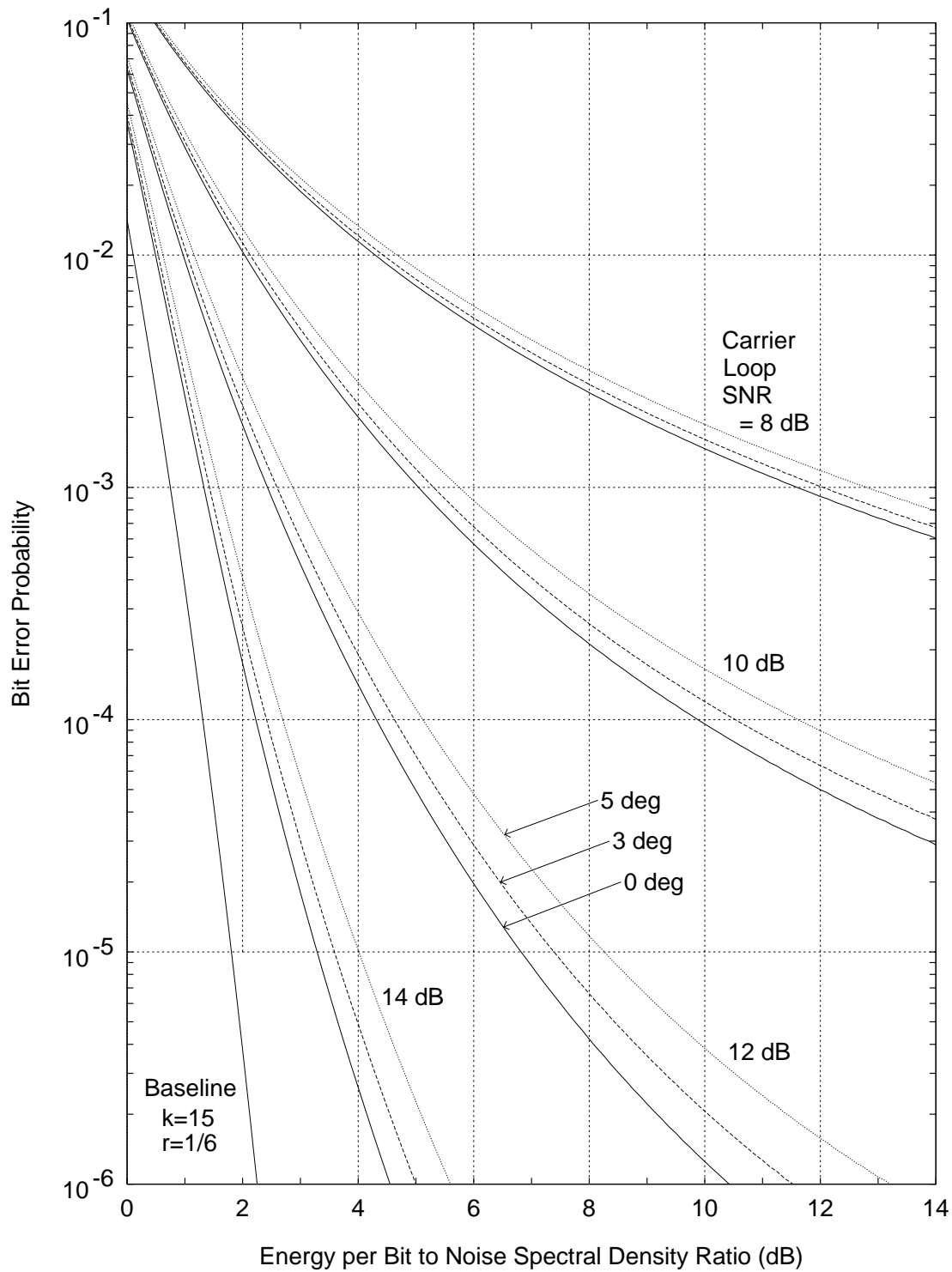


Figure 14: Optimum Modulation Index; Uncoded

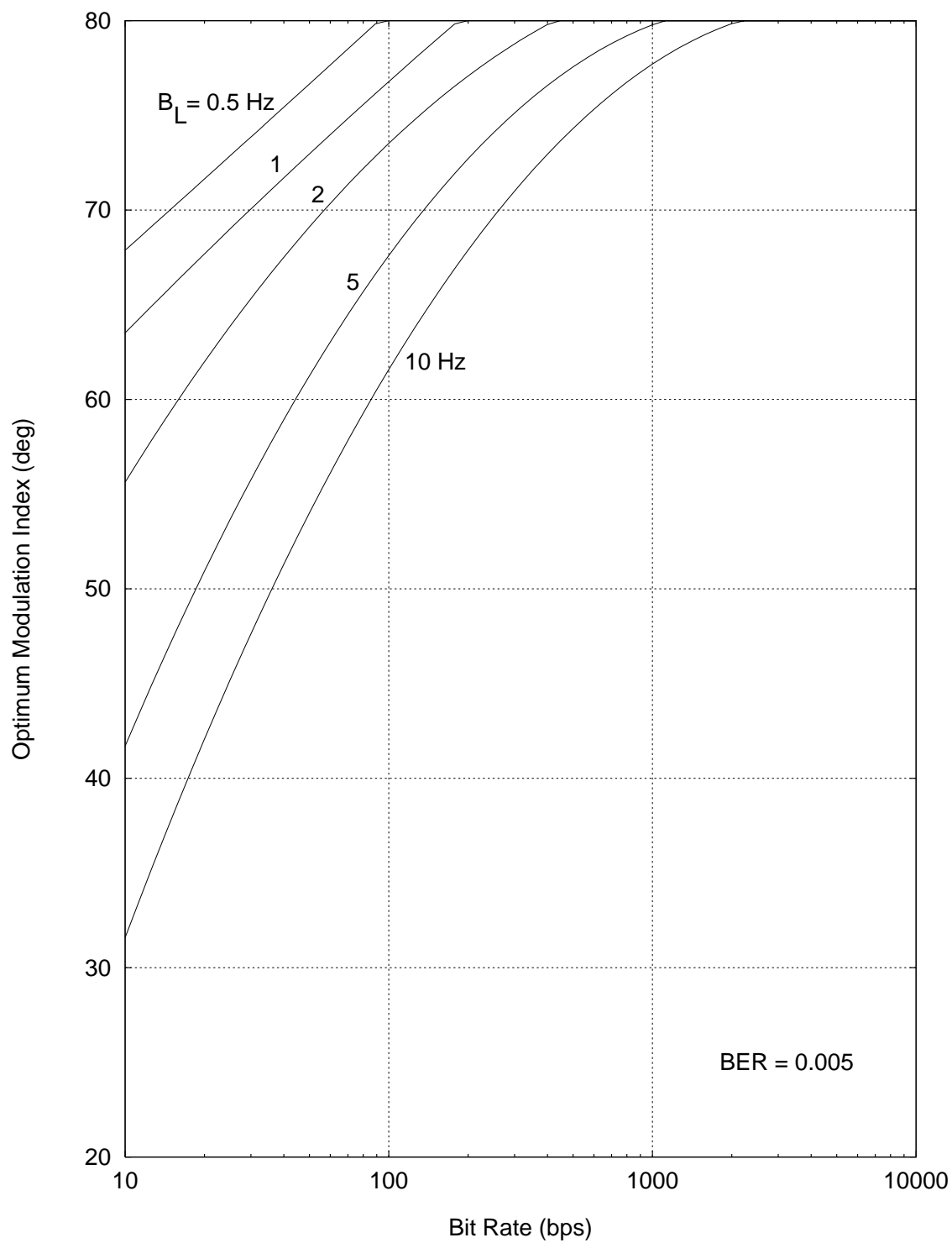


Figure 15: Optimum Modulation Index; Conv. Code (k=7, r=1/2)

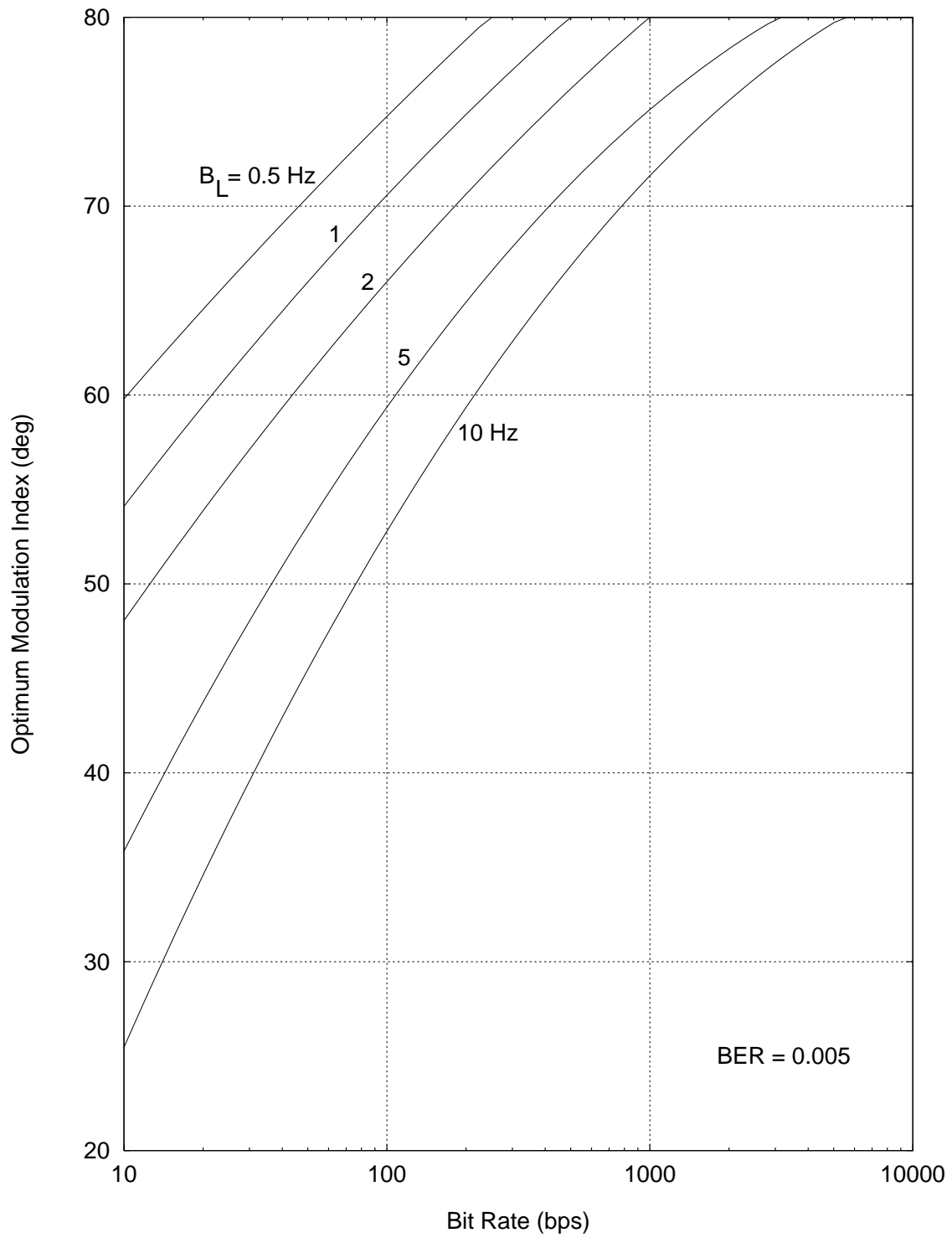
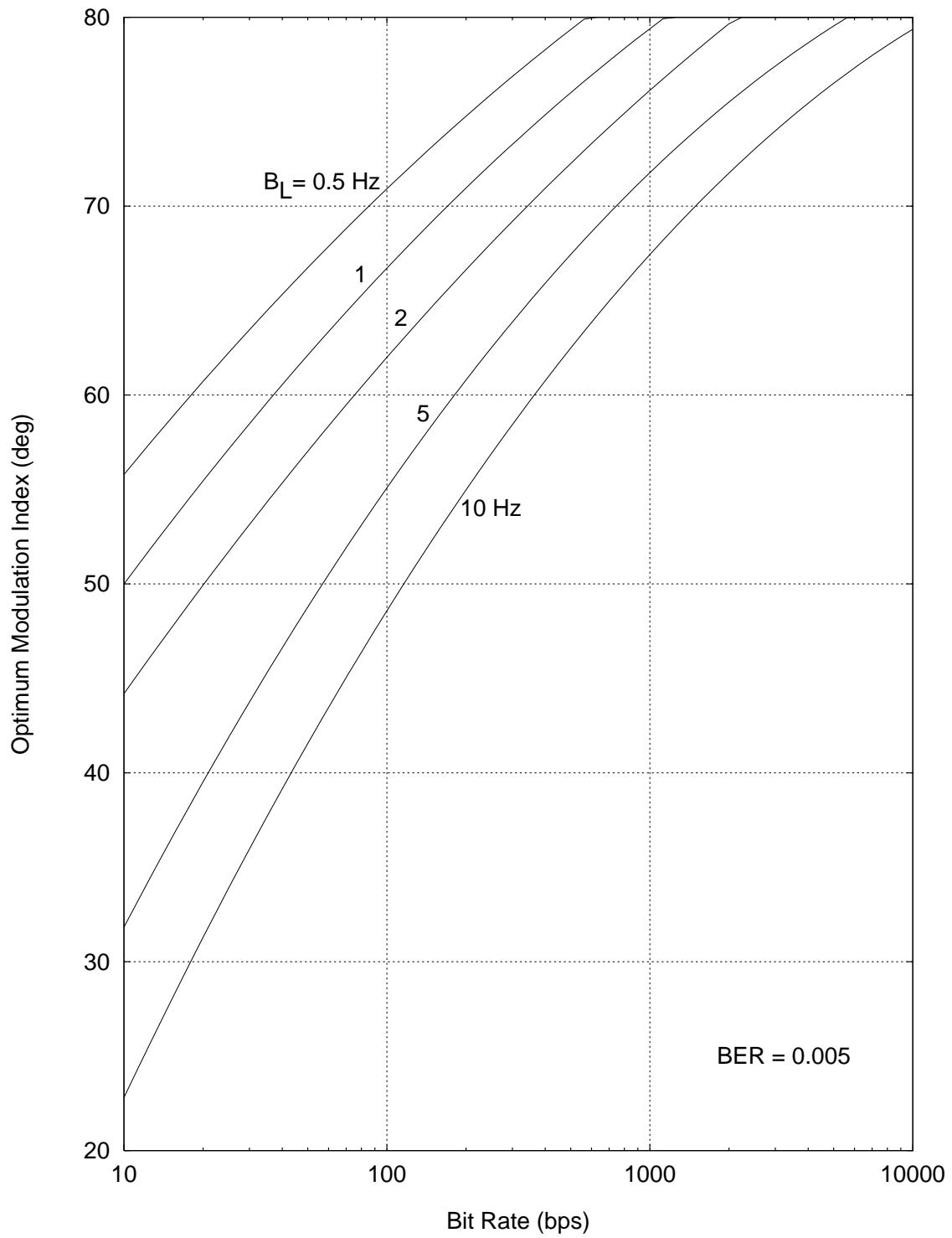


Figure 16: Optimum Modulation Index; Conv. Code (k=15, r=1/4)



To good approximation, the optimum modulation indices of Figure 16 may also be used for a concatenated Reed-Solomon (255, 223) / convolutional ($k = 15, r = 1/4$) code with an end-to-end threshold BER of 10^{-5} . In addition, this same figure may be used for a concatenated Reed-Solomon (255, 223) / convolutional ($k = 15, r = 1/6$) code.

Sometimes, it is important to take transmitter and solar phase noise into account. This is especially true for operation close to the sun or for one-way or two-way noncoherent operation with an Auxiliary Oscillator (or some oscillator, serving as the source of the downlink carrier, that has relatively poor frequency stability).

Radio loss may, more generally, be regarded as a function of the carrier phase error variance σ_ϕ^2 .

$$\sigma_\phi^2 = \frac{1}{\rho_L} + \sigma_T^2 + \sigma_S^2 \quad \text{rad}^2 \quad (20)$$

σ_T^2 is the contribution of the transmitter phase noise to the phase error variance in the carrier loop and σ_S^2 is the contribution of solar phase noise. σ_T^2 is a function of B_L and the statistical properties of the transmitter phase noise. Appendix D offers suggestions for estimating σ_T^2 . If the sun-earth-probe angle is small, σ_S^2 will be significant and must be taken into account. Appendix E provides estimates of σ_S^2 as a function of sun-earth-probe angle and B_L .

In general, as a first step in estimating radio loss, the carrier phase error variance σ_ϕ^2 should be calculated using equation (20). Then radio loss will be calculated as a function of σ_ϕ^2 . Appendix B provides the details.

It is recommended that the following constraint on residual-carrier tracking be observed.

$$\sigma_\phi^2 \leq 0.10 \text{ rad}^2 \quad (21)$$

In the absence of transmitter or solar phase noise, this becomes $\rho_L \geq 10.0$ (10 dB). In general, with transmitter or solar phase noise present, ρ_L needs to be larger yet.

Figure 17 shows the high-rate model radio loss for residual-carrier tracking of uncoded telemetry. Figures 18 and 19 show the high-rate model radio loss for residual-carrier tracking of convolutionally coded ($k = 7, r = 1/2$) and ($k = 15, r = 1/4$) telemetry, respectively. Since the performance of the rate 1/6 convolutional code is close to that of the rate 1/4 code, the radio loss for the ($k = 15, r = 1/6$) code is well approximated by the curves of Figure 19.

Figure 17: Radio Loss (HRM); Uncoded, Residual Carrier

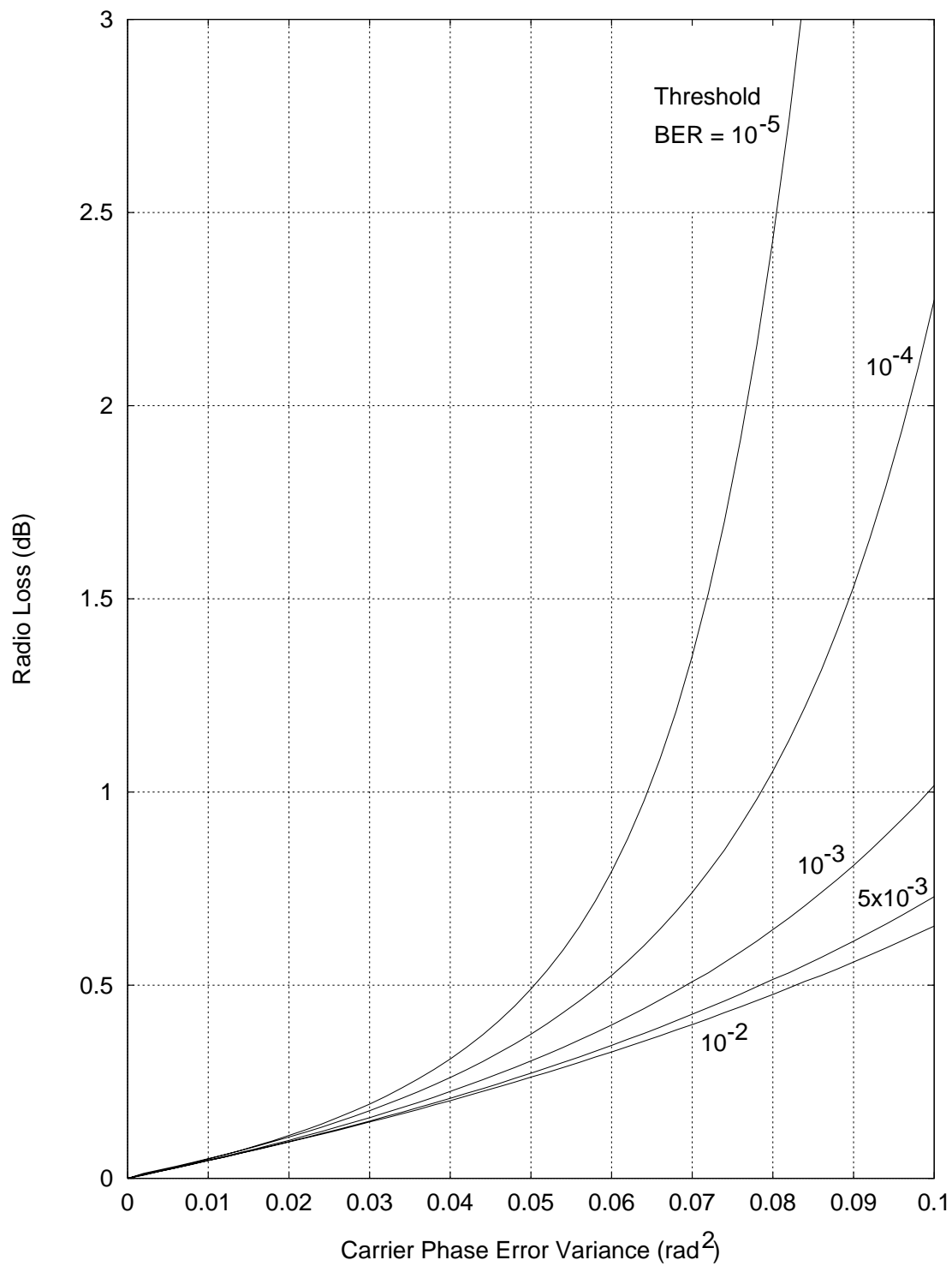


Figure 18: Radio Loss (HRM); Conv. Code ($k=7$, $r=1/2$), Residual Carrier

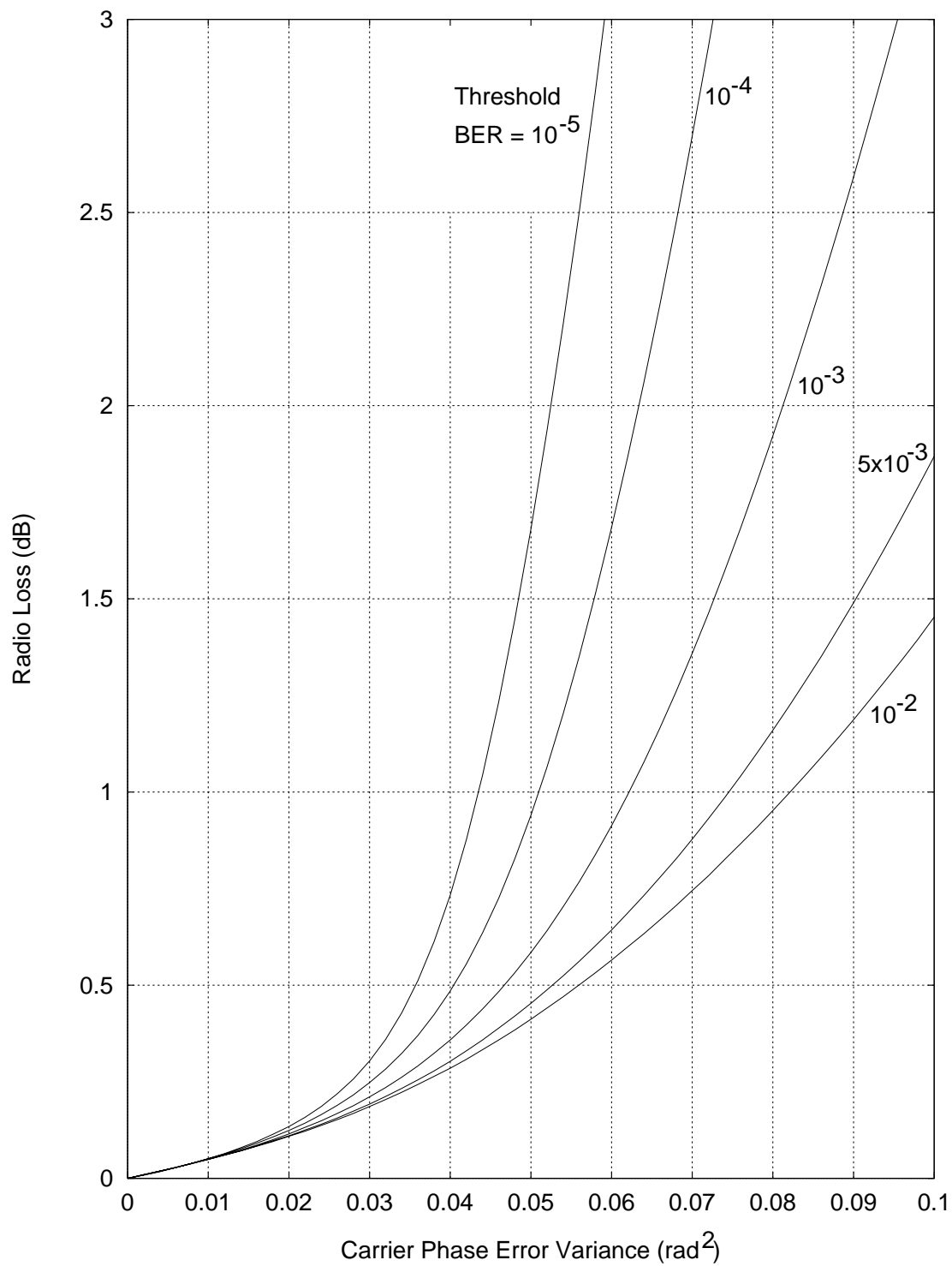
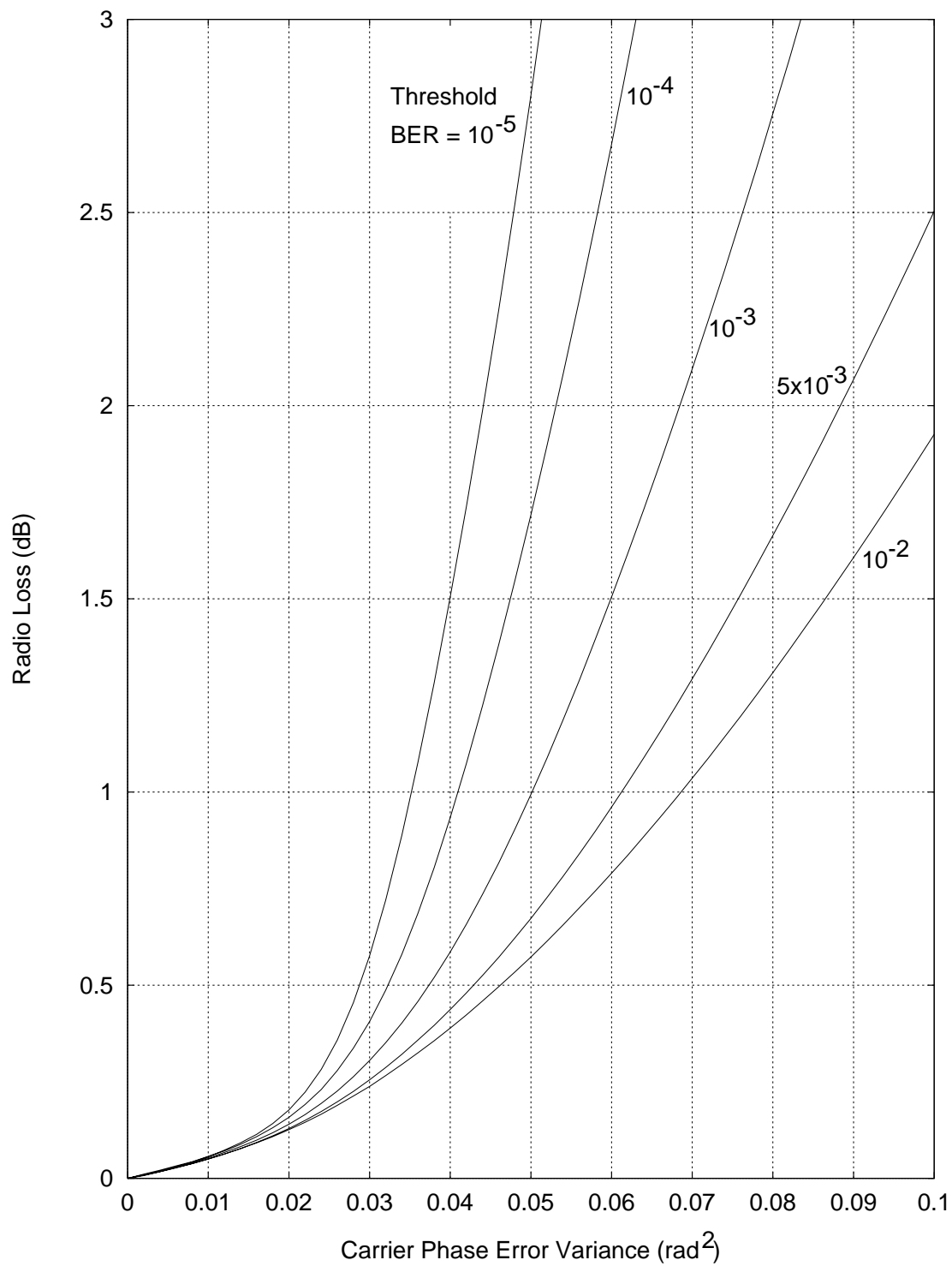


Figure 19: Radio Loss (HRM); Conv. Code (k=15, r=1/4), Residual Carrier



The 5×10^{-3} BER radio loss curve of Figure 18 may also be used as an estimate of radio loss for a concatenated Reed-Solomon (255, 223) / convolutional ($k = 7, r = 1/2$) code with an end-to-end threshold BER of 10^{-5} .

The 5×10^{-3} BER radio loss of Figure 19 may also be used for as an estimate of radio loss for a concatenated Reed-Solomon (255, 223) / convolutional ($k = 15, r = 1/4$) code with an end-to-end threshold BER of 10^{-5} . In addition, this same curve may be used for a concatenated Reed-Solomon (255, 223) / convolutional ($k = 15, r = 1/6$) code.

Appendix B contains exponential approximations to the curves of Figures 17 through 19.

2.4.3.2 *Suppressed Carrier*

A suppressed carrier is tracked with a Costas loop. This loop has different statistical properties than does the residual-carrier loop; thus, radio loss will be different in this case. Appendix B summarizes the models.

When tracking a suppressed carrier, the carrier loop signal-to-noise ratio is

$$\rho_L = \frac{S_L P_T}{N_0 B_L} \quad (22)$$

where S_L is the squaring loss of the Costas loop (Reference 5).

$$S_L = \frac{2 \frac{E_s}{N_0}}{1 + 2 \frac{E_s}{N_0}} \quad (23)$$

Radio loss is a function of the carrier phase error variance σ_ϕ^2 .

$$\sigma_\phi^2 = \frac{1}{\rho_L} + \sigma_T^2 + \sigma_s^2 \quad \text{rad}^2 \quad (24)$$

As before, σ_T^2 and σ_s^2 are the contributions of transmitter and solar phase noise, respectively, to the phase error variance in the carrier loop (see Appendices D and E).

Figure 20 shows the high-rate model radio loss for suppressed-carrier tracking of uncoded telemetry. Figures 21 and 22 show the high-rate model radio loss for suppressed-carrier tracking of convolutionally coded ($k = 7, r = 1/2$) and ($k = 15, r = 1/4$) telemetry, respectively. Since the performance of the rate 1/6 convolutional code is close

to that of the rate 1/4 code, the radio loss for the $(k=15, r=1/6)$ code is well approximated by the curves of Figure 22.

The 5×10^{-3} BER radio loss curve of Figure 21 may also be used as an estimate of radio loss for a concatenated Reed-Solomon (255, 223) / convolutional $(k=7, r=1/2)$ code with an end-to-end threshold BER of 10^{-5} .

The 5×10^{-3} BER radio loss of Figure 22 may also be used for as an estimate of radio loss for a concatenated Reed-Solomon (255, 223) / convolutional $(k=15, r=1/4)$ code with an end-to-end threshold BER of 10^{-5} . In addition, this same curve may be used for a concatenated Reed-Solomon (255, 223) / convolutional $(k=15, r=1/6)$ code.

Even though each of Figures 20 through 22 has a horizontal axis that extends to 0.05 rad^2 , operation beyond 0.02 rad^2 is not recommended.

$$\sigma_{\phi}^2 \leq 0.02 \text{ rad}^2 \quad (25)$$

Violating this recommendation will lead to (at least) an occasional half-cycle slip. In the absence of transmitter or solar phase noise, inequality (25) corresponds to $\rho_L \geq 50.0$ (17 dB). See Reference 6. In general, with transmitter or solar phase noise present, ρ_L needs to be larger yet.

Appendix B contains exponential approximations for suppressed carrier radio loss.

2.4.3.3 *Two-Way Coherent*

Radio loss for two-way coherent operation may be approximated by using the same curves as for one-way tracking, but using a modified carrier phase error variance.

When the spacecraft is tracked in a two-way phase-coherent mode, the carrier phase error variance σ_{ϕ}^2 in the ground receiver is increased by a portion of the phase noise (of thermal origin) introduced on the downlink by the spacecraft transponder.

$$\sigma_{\phi}^2 = \frac{1}{\rho_L} + \frac{G^2(B_{TR} - B_L)}{P_C/N_0|_{U/L}} + \sigma_s^2 \text{ rad}^2 \quad (26)$$

where G is the spacecraft transponder ratio and $P_C/N_0|_{U/L}$ is the uplink residual carrier power to noise spectral density ratio. B_{TR} and B_L are the (one-sided) noise-equivalent carrier loop bandwidths of the transponder and ground receiver, respectively.

Figure 20: Radio Loss (HRM); Uncoded, Suppressed Carrier

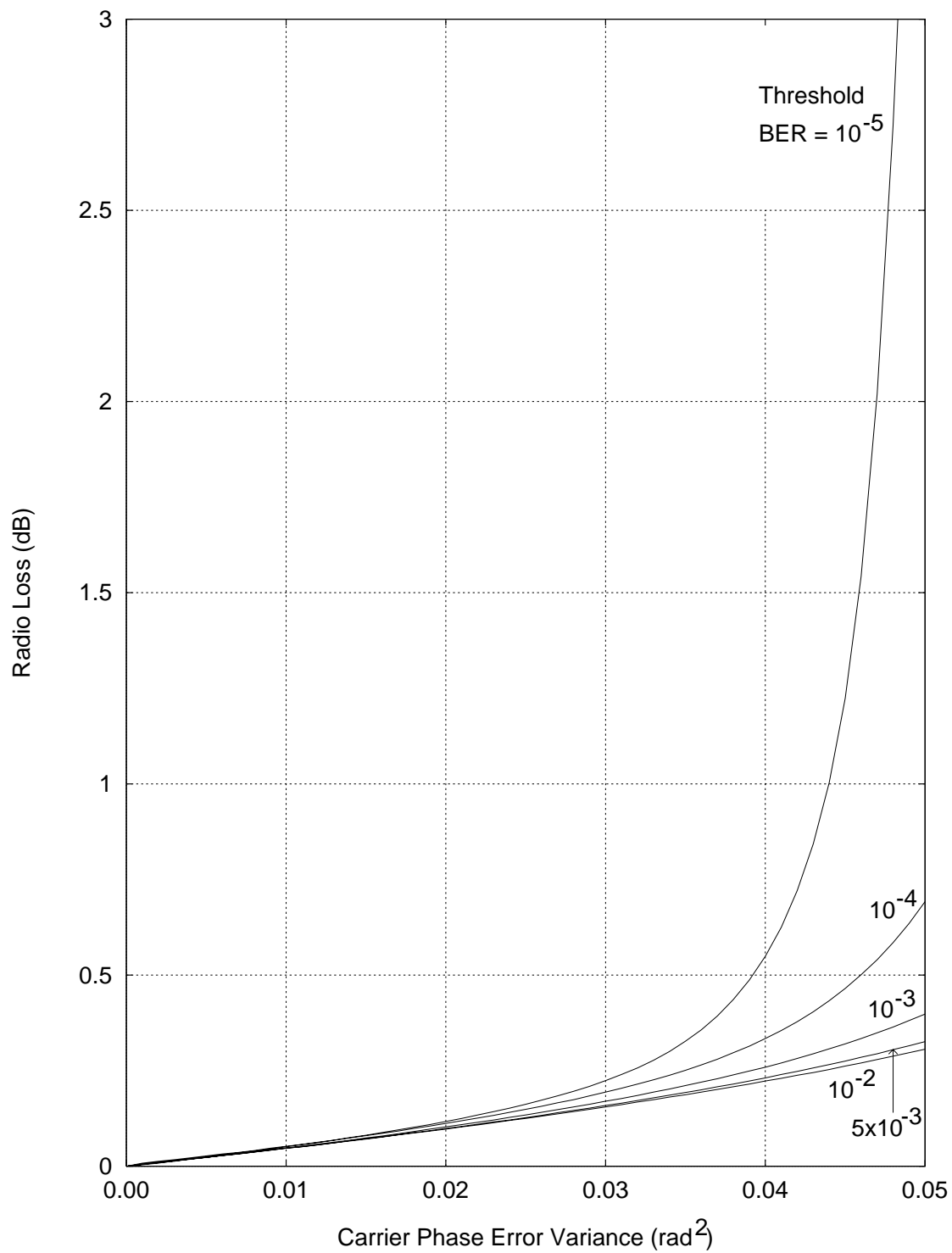


Figure 21: Radio Loss (HRM); Conv. Code ($k=7$, $r=1/2$), Suppressed Carrier

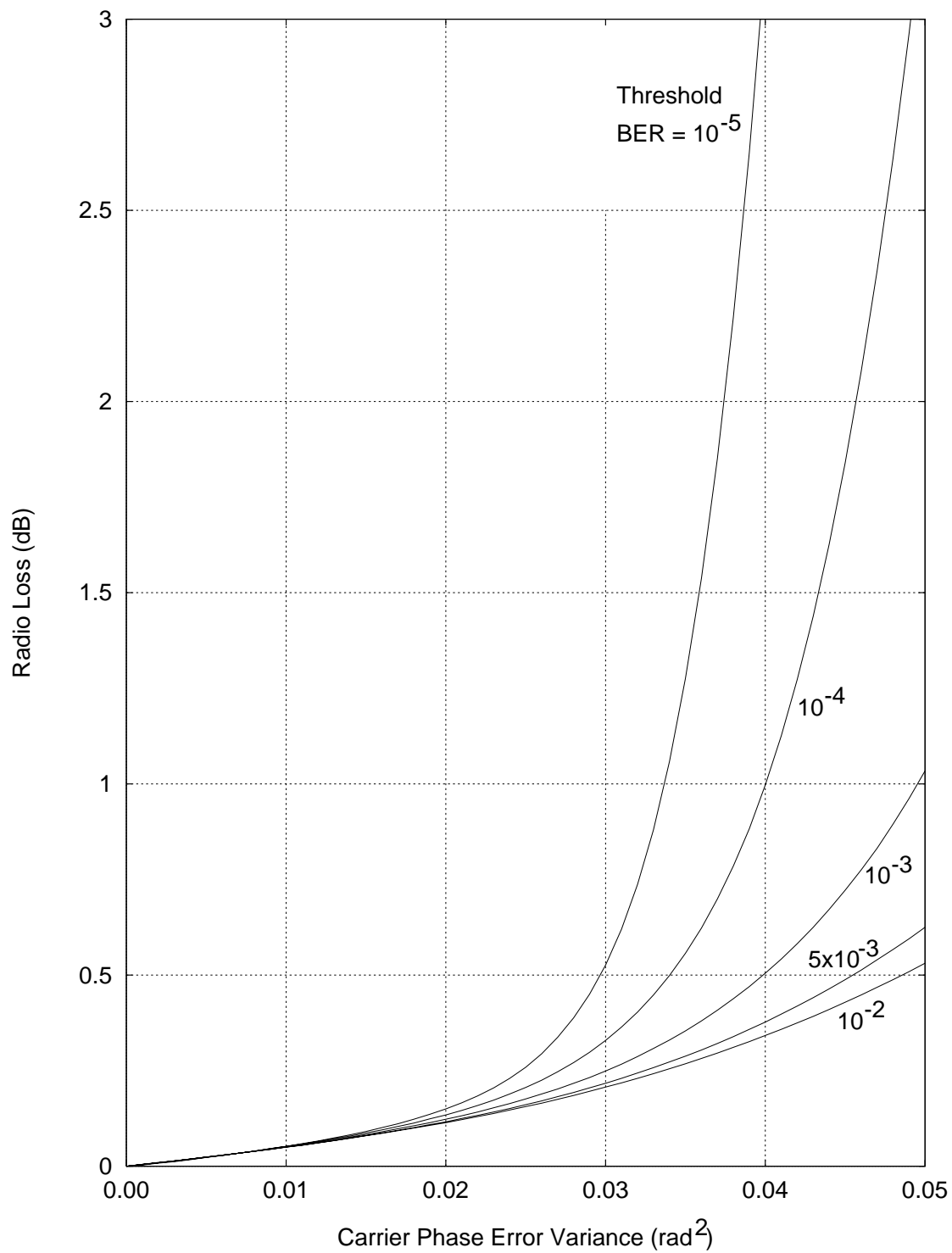
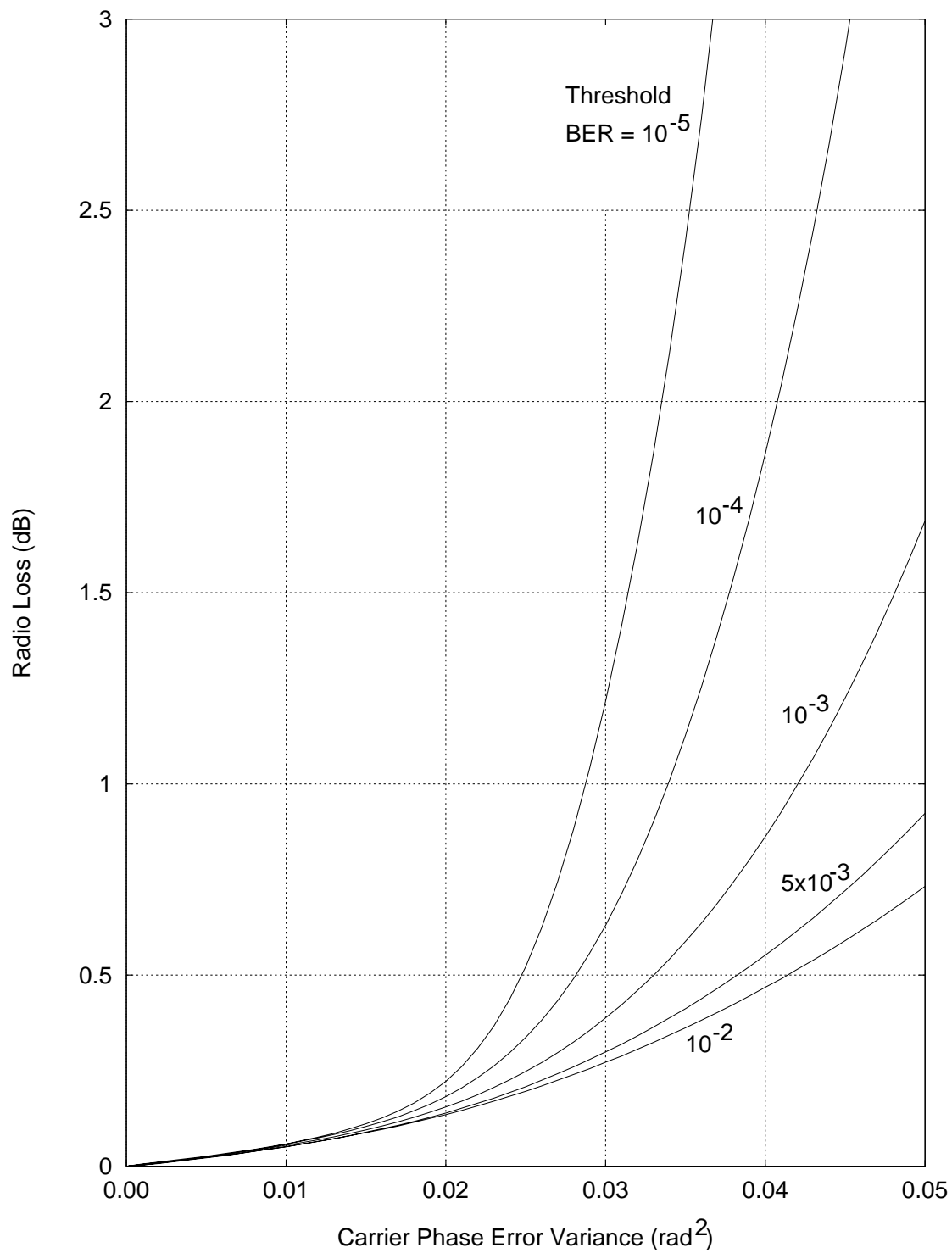


Figure 22: Radio Loss (HRM); Conv. Code (k=15, r=1/4), Suppressed Carrier



Equation (26) is a valid approximation only if $B_{TR} > B_L$. σ_s^2 is the contribution of solar phase noise to the phase error variance in the carrier loop; it will generally be larger for two-way coherent operation than for one-way or two-way noncoherent operation (see Appendix E).

Figure 23 shows an example of two-way coherent radio loss. In that figure both uplink and downlink are residual carrier and X-band. A convolutional ($k = 15, r = 1/4$) code is used with threshold BER of 5×10^{-3} . The solar phase noise contribution is negligible, and B_{TR} is much larger than B_L . The figure shows how two-way coherent radio loss depends on the uplink and downlink carrier loop signal-to-noise ratios.

2.4.4 Subcarrier Synchronization

Subcarrier demodulation loss η_{SUB} ($0 < \eta_{SUB} \leq 1$) is a contributor to system loss. It is the result of imperfect subcarrier synchronization. In general, the subcarrier demodulation loss is a function of subcarrier loop signal-to-noise ratio, the coding scheme, the threshold BER, and the type of subcarrier (squarewave or sinewave).

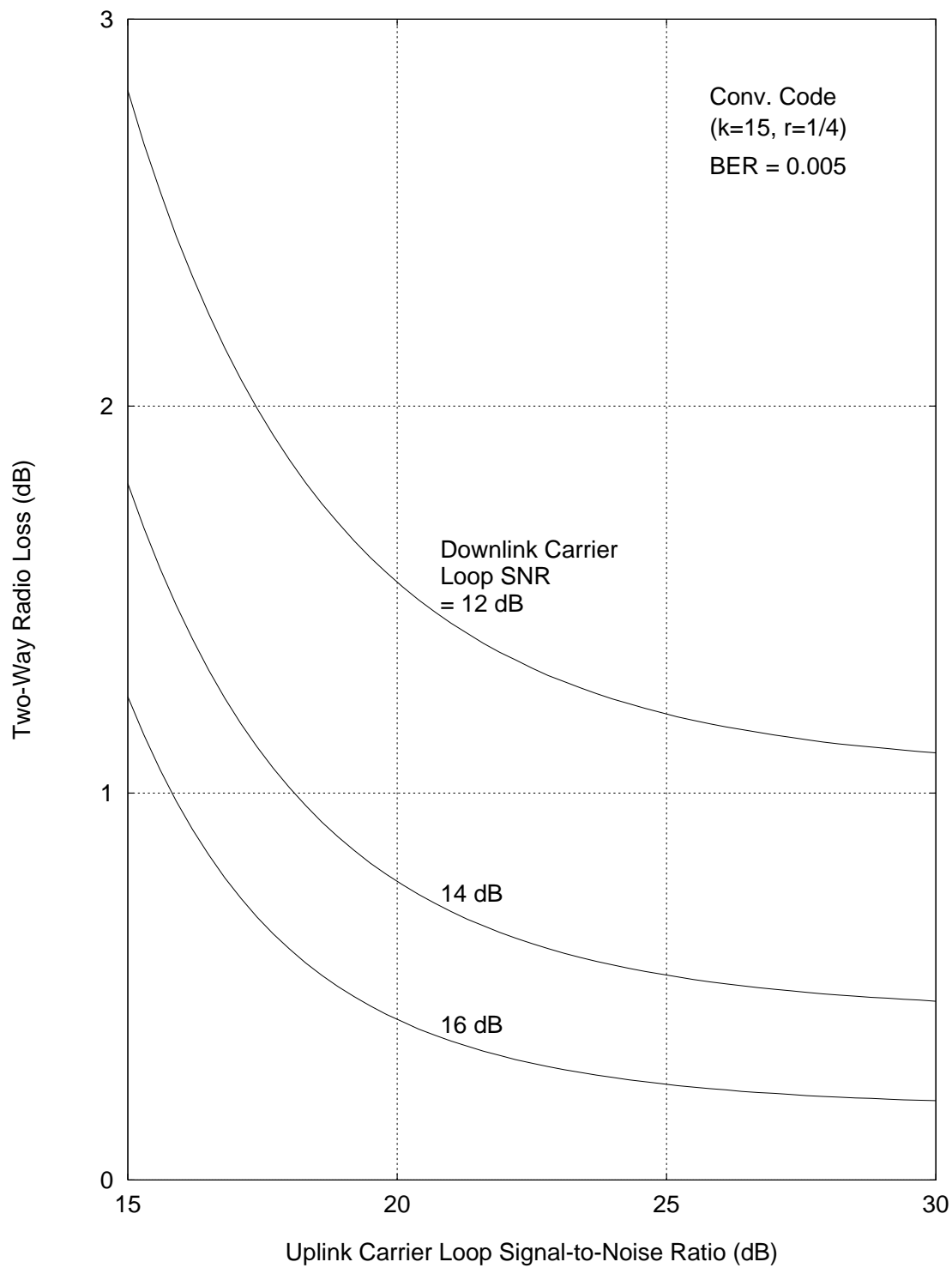
The signal-to-noise ratio ρ_{SUB} in a subcarrier synchronization loop is given by (Reference 7)

$$\rho_{SUB} = \begin{cases} \left(\frac{2}{\pi}\right)^2 \cdot \frac{S_{SUB}}{W_{SUB} B_{SUB}} \cdot \frac{P_D}{N_0}, & \text{squarewave subcarrier} \\ \frac{S_{SUB}}{B_{SUB}} \cdot \frac{P_D}{N_0}, & \text{sinewave subcarrier} \end{cases} \quad (27)$$

B_{SUB} is the (one-sided) noise-equivalent subcarrier loop bandwidth. S_{SUB} is the squaring loss of the subcarrier loop. For a squarewave subcarrier, P_D is the power in all the data modulation sidebands; whereas for a sinewave subcarrier, P_D is the power in the fundamental data modulation sidebands only. For a squarewave subcarrier, W_{SUB} is the subcarrier loop window factor ($W_{SUB} = 2^{-n}$, where $n = 0, 1, 2, 3$, or 4). A window is not used with sinewave subcarriers. The squaring loss S_{SUB} is, in the case of either squarewave or sinewave,

$$S_{SUB} = \frac{2 \frac{E_s}{N_0}}{1 + 2 \frac{E_s}{N_0}} \quad (28)$$

Figure 23: Two-Way Radio Loss (HRM); Residual Carrier, X-up/X-down



It is recommended that the following constraint on subcarrier tracking be observed.

$$\rho_{SUB} \geq 100.0 \text{ (20 dB)} \quad (29)$$

Figure 24 shows subcarrier demodulation loss for a squarewave subcarrier as a function of ρ_{SUB} for uncoded telemetry. As is evident from this figure, the dependence on threshold BER is rather mild. Figures 25 and 26 shows subcarrier demodulation loss for a squarewave subcarrier as a function of ρ_{SUB} for convolutionally coded ($k = 7, r = 1/2$) and ($k = 15, r = 1/4$) telemetry. Since the performance of the rate 1/6 convolutional code is close to that of the rate 1/4 code, the subcarrier demodulation loss for the ($k = 15, r = 1/6$) code is well approximated by the curves of Figure 26.

Appendix F summarizes the subcarrier demodulation loss models. Exponential approximations are given there.

2.4.5 *Symbol Synchronization*

Imperfect symbol synchronization results in a finite symbol synchronization loss η_{SYM} ($0 < \eta_{SYM} \leq 1$), which is a contributor to system loss. The symbol synchronization loss is a function of symbol loop signal-to-noise ratio.

The signal-to-noise ratio ρ_{SYM} in the symbol synchronization loop is given by (Reference 8)

$$\rho_{SYM} = \frac{2}{(2\pi)^2} \cdot \frac{S_{SYM}}{W_{SYM} B_{SYM}} \cdot \frac{P_D}{N_0} \quad (30)$$

where B_{SYM} is the (one-sided) noise-equivalent symbol loop bandwidth, W_{SYM} is the symbol loop window factor ($W_{SYM} = 2^{-n}$, where $n = 0, 1, 2, 3$, or 4), and S_{SYM} is the squaring loss of the symbol loop. S_{SYM} takes on values from 0 to 1 and asymptotically equals 1 for large values of E_s/N_0 . Figure 27 shows S_{SYM} (dB) as a function of E_s/N_0 . Appendix G gives equations for calculating S_{SYM} .

It is recommended that the following constraint on symbol synchronization be observed.

$$\rho_{SYM} \geq 31.6 \text{ (15 dB)} \quad (31)$$

The inequality (31) is based on the assumption that the symbol transition density is approximately 0.5 or higher. If the symbol transition density is closer to 0.25, then it is recommended that ρ_{SYM} be at least 18 dB.

Figure 24: Squarewave Subcarrier Demodulation Loss; Uncoded

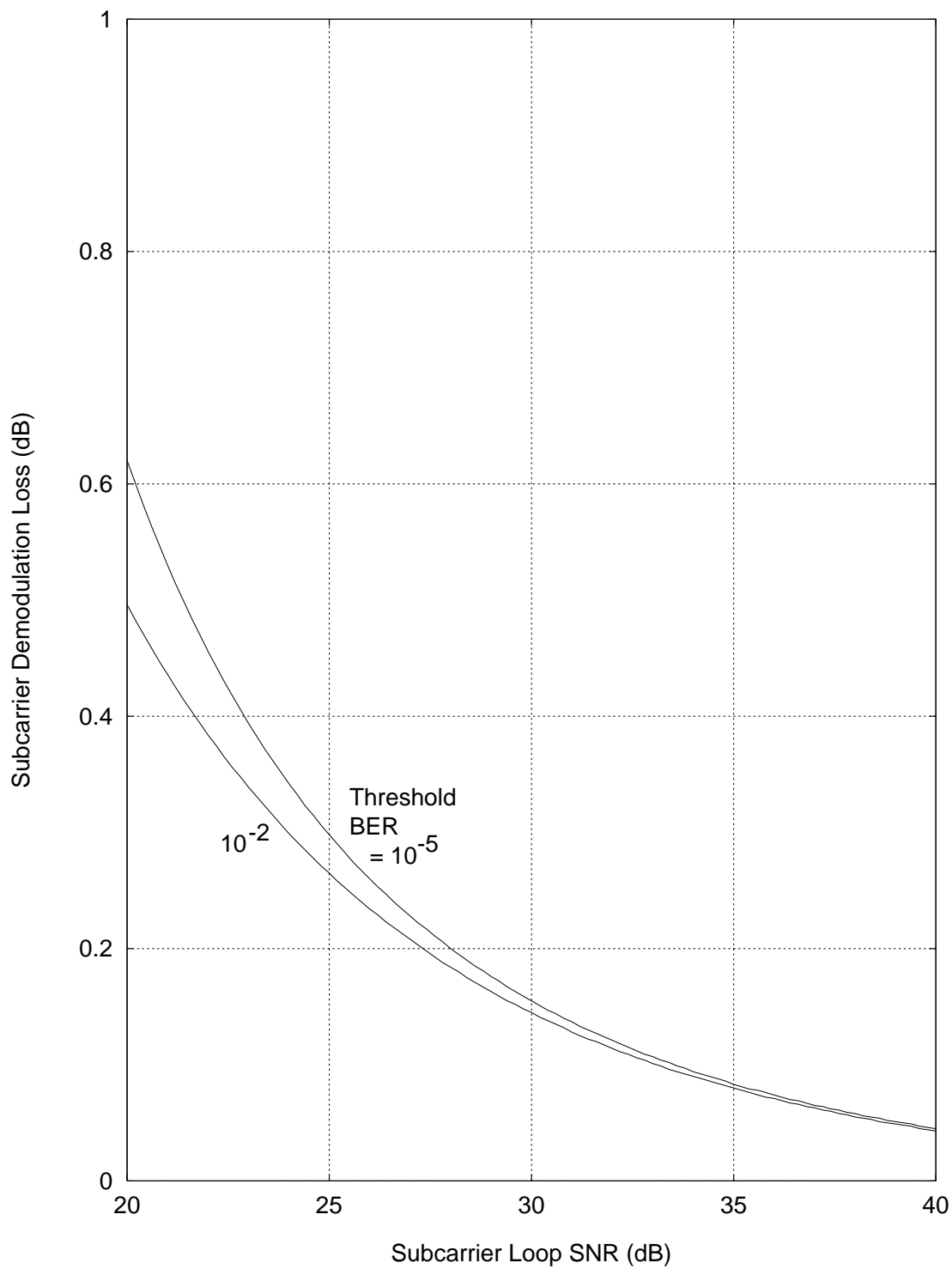


Figure 25: Squarewave Subcarrier Demodulation Loss; Conv. Code (k=7, r=1/2)

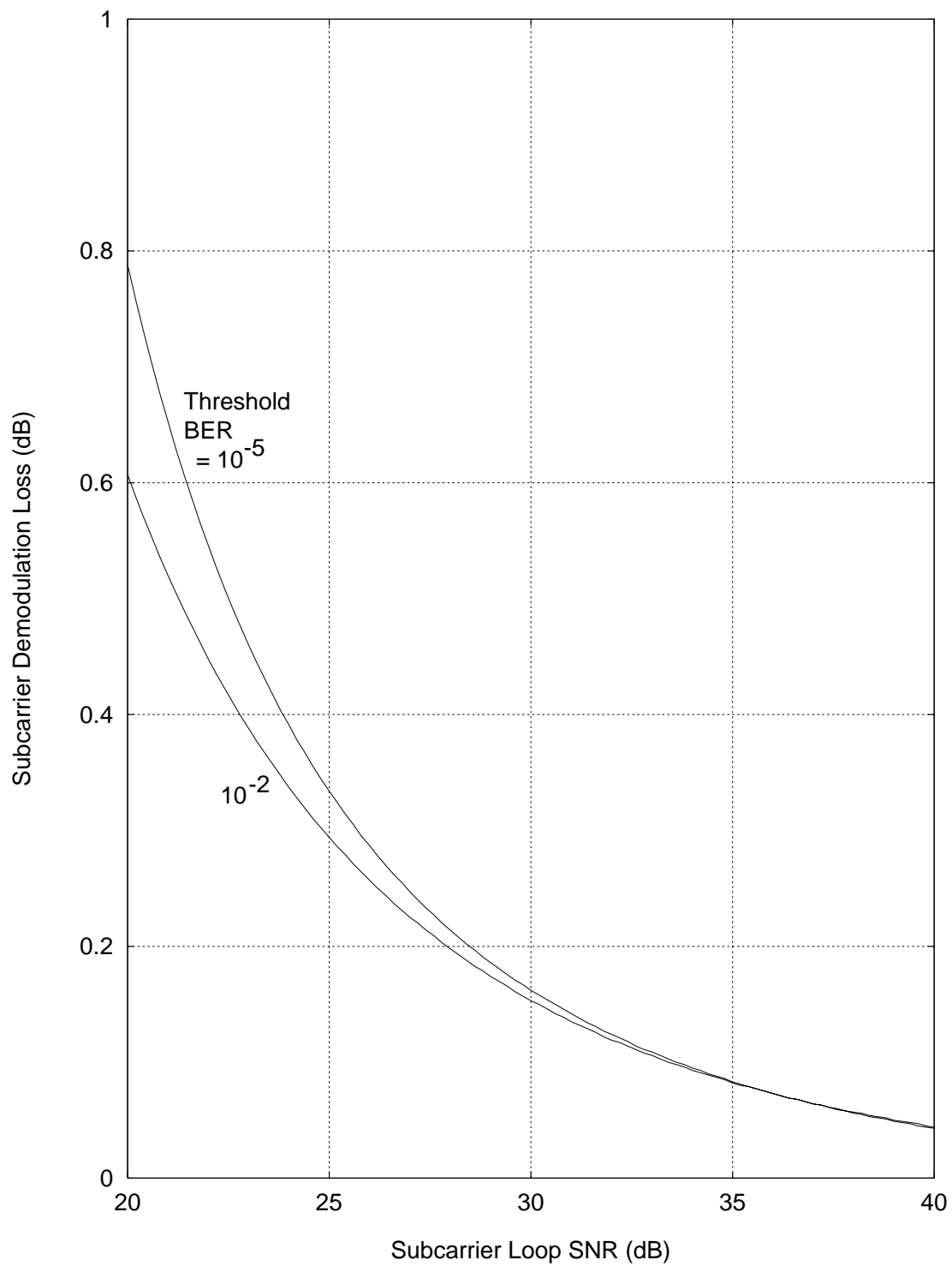


Figure 26: Squarewave Subcarrier Demodulation Loss; Conv. Code (k=15, r=1/4)

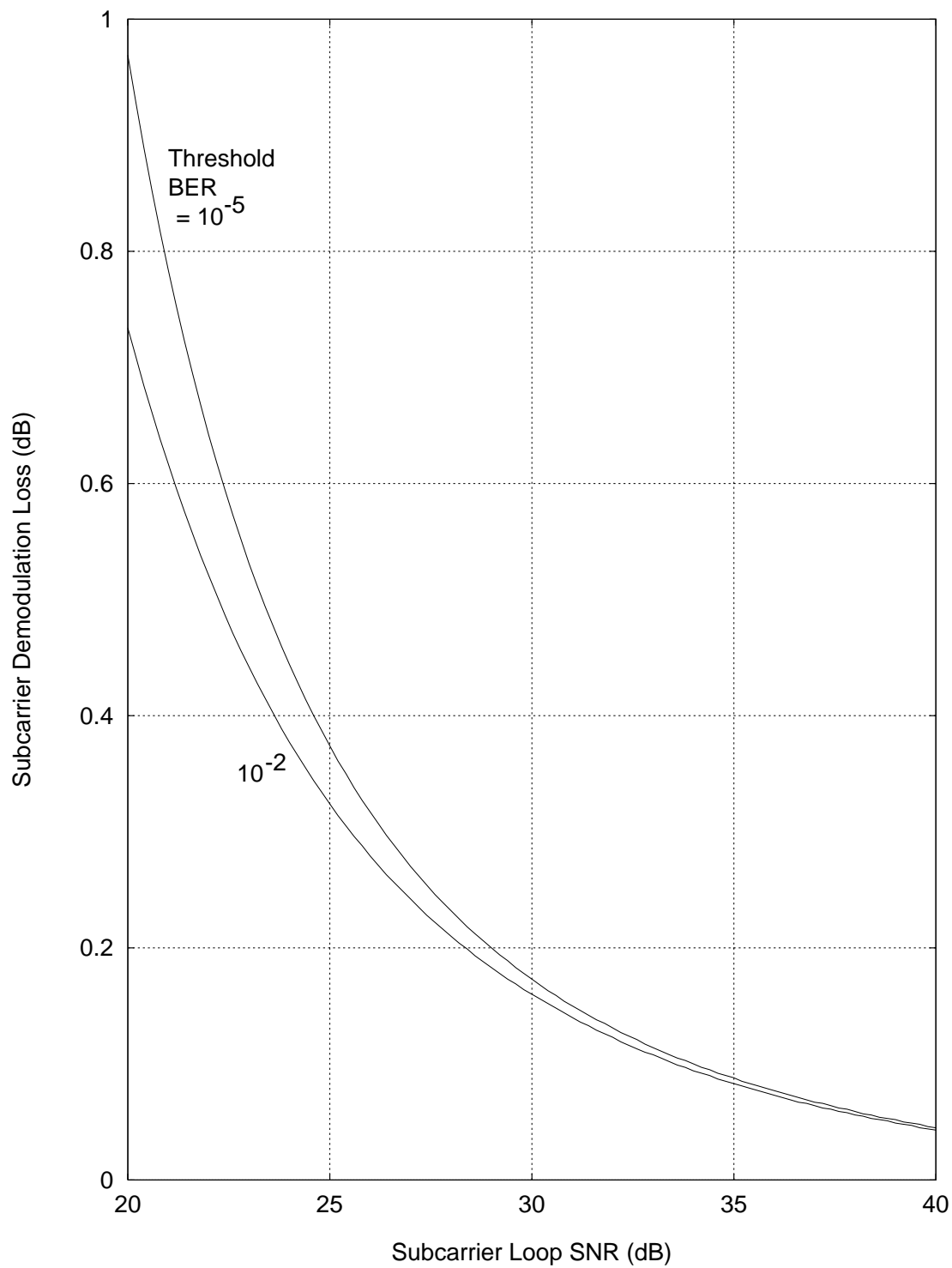
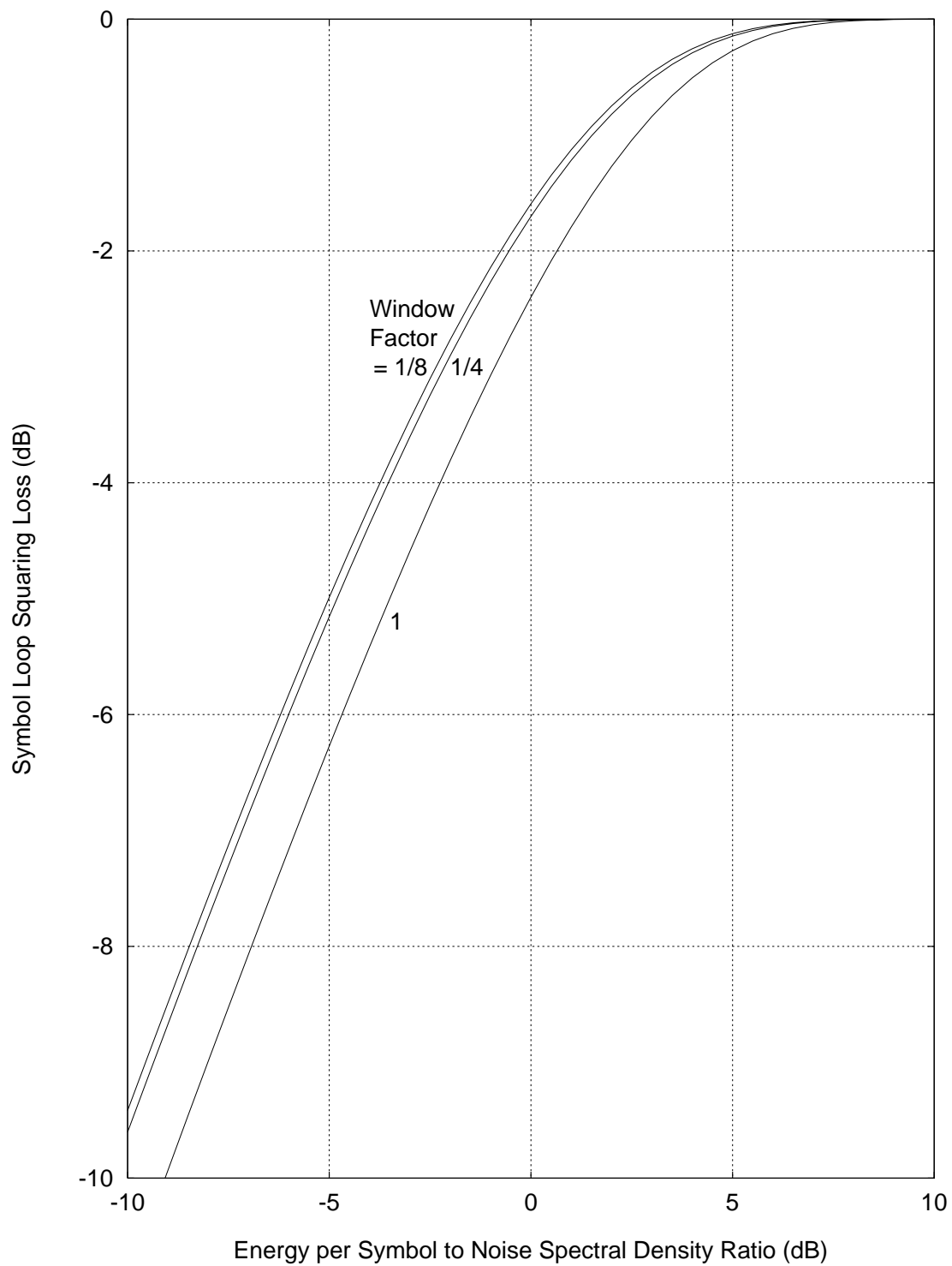


Figure 27: Symbol Loop Squaring Loss



η_{SYM} is approximately the same for all coding schemes and threshold BERs of interest. Figure 28 shows symbol synchronization loss as a function of ρ_{SYM} . Appendix H summarizes the model and gives exponential approximations.

2.4.6 *Waveform Distortion*

Deviations of either the subcarrier waveform or the symbol waveform from ideal will adversely affect telemetry performance. In general, waveform distortion loss η_{WD} (fractional and dimensionless) is the composite loss factor that incorporates both of these deviations. η_{WD} , in turn, is a contributor to the system loss η_{SYS} .

In the case of no subcarrier, only the symbol waveform deviation is of concern.

$$\eta_{WD} = 1 - 2 \cdot \left(\frac{\Delta T_{SYM}}{T_{SYM}} \right) + 2 \cdot \left(\frac{\Delta T_{SYM}}{T_{SYM}} \right)^2 \quad (32)$$

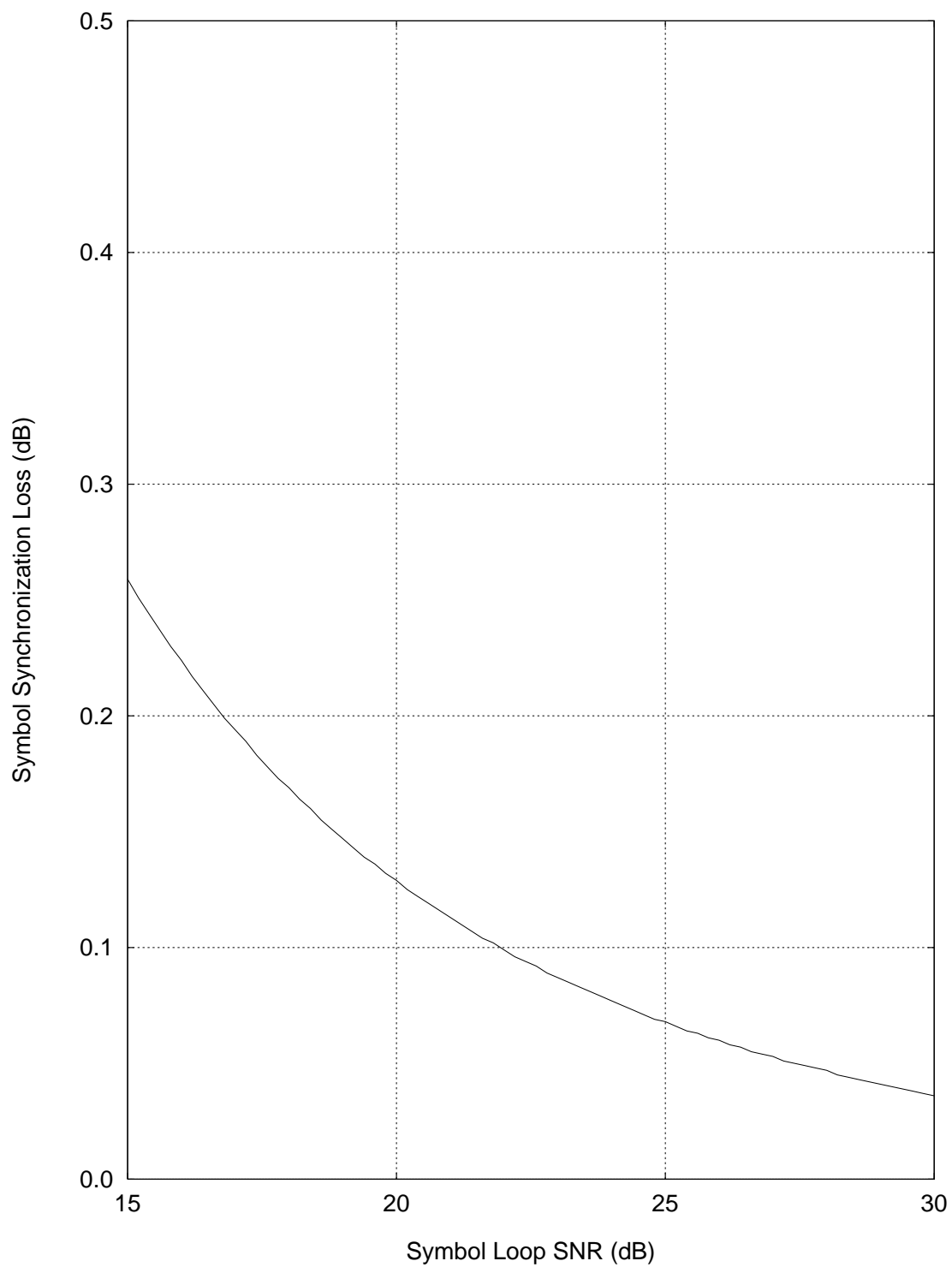
T_{SYM} is the symbol period in seconds and ΔT_{SYM} its asymmetry. It is recommended that the rise and fall times (10 to 90 percent points) of the symbol waveform be equal to or less than 1 percent of the symbol period and that asymmetry be equal to or less than 2 percent.

In the case of a squarewave subcarrier,

$$\eta_{WD} = \left[1 - \frac{2\Delta T_{SUB}}{T_{SUB}} \right]^2 \cdot \left[1 - 2 \cdot \left(\frac{\Delta T_{SYM}}{T_{SYM}} \right) + 2 \cdot \left(\frac{\Delta T_{SYM}}{T_{SYM}} \right)^2 \right] \quad (33)$$

T_{SUB} is the subcarrier period in seconds and ΔT_{SUB} its asymmetry.

Figure 28: Symbol Synchronization Loss



Appendix A *Ideal Functional Dependence of BER on E_b/N_0*

The functional dependence of BER on bit SNR, E_b/N_0 , in the ideal case of no system loss (i.e., with a system loss of 0 dB) is here denoted

$$\text{Baseline:} \quad \text{BER} = f(E_b/N_0) \quad (\text{A-1})$$

This performance is never achieved in practice. Nonetheless, this idealized performance is a useful reference (baseline) from which to measure actual performance. For uncoded telemetry,

$$f(x) = \frac{1}{2} \text{erfc}(\sqrt{x}) \quad (\text{A-2})$$

where

$$\text{erfc}(x) = 1 - \text{erf}(x) = 1 - \frac{2}{\sqrt{\pi}} \int_0^x e^{-y^2} dy \quad (\text{A-3})$$

For convolutionally coded telemetry, the baseline telemetry performance is approximated as

$$f(x) = \min \left\{ \frac{1}{2}, \exp(a_0 - a_1 x) \right\} \quad (\text{A-4})$$

where the coefficients a_0 and a_1 depend on the particular convolutional code, as indicated in Table A-1.

Table A-1: Coefficients a_0 and a_1 for Equation (A-4)

| Code | a_0 | a_1 |
|---------------------|--------|--------|
| ----- | ---- | ---- |
| $(k = 7, r = 1/2)$ | 4.4514 | 5.7230 |
| $(k = 15, r = 1/4)$ | 9.8070 | 13.431 |
| $(k = 15, r = 1/6)$ | 9.8070 | 14.064 |

Appendix B Radio Loss

Three different models for radio loss are summarized in this appendix: the High-Rate Model (HRM), the Low-Rate Model (LRM), and the Medium-Rate Model (MRM). When the symbol rate is much larger than the carrier loop bandwidth, radio loss may be accurately predicted with the HRM; this model will, therefore, be valid for many applications of the Block-V Receiver. When the symbol rate is much smaller than the carrier loop bandwidth, radio loss may be predicted with the LRM; however, the symbol rate is rarely this small. The common use of the LRM is as a component, along with the HRM, in an interpolation that is intended to model radio loss in those cases for which the symbol rate is not much larger than the carrier loop bandwidth (Reference 9). This interpolation is called the MRM.

B.1 High-Rate Model (HRM)

The HRM for radio loss is valid when the symbol rate is much larger than B_L . For smaller symbol rates, it gives pessimistic results. The HRM radio loss, η_{HRM} (fractional and dimensionless), is given by

$$\eta_{HRM} = \frac{f^{-1}(\text{BER})}{E_b/N_0} \quad (\text{B-1})$$

where $f(\cdot)$ is the ideal functional dependence of probability of bit error on bit SNR (see Appendix A), corresponding to zero decibels of system loss. In the above equation (B-1) E_b/N_0 is the actual bit SNR needed to achieve a given threshold BER in the presence of imperfect carrier synchronization; it is the solution of the following equation

$$\text{BER} = \int_{-\pi/2}^{\pi/2} f\left(\frac{E_b}{N_0} \cos^2 \phi\right) p_\phi(\phi) d\phi \quad (\text{B-2})$$

where $p_\phi(\phi)$ is the probability density function of the carrier loop phase error ϕ and BER is, as before, the threshold bit error rate. When tracking a residual carrier,

$$p_\phi(\phi) = \frac{\exp\left[\frac{\cos \phi}{\sigma_\phi^2}\right]}{\int_{-\pi/2}^{\pi/2} \exp\left[\frac{\cos \psi}{\sigma_\phi^2}\right] d\psi}, \quad |\phi| \leq \pi/2 \quad (\text{B-3})$$

When tracking a suppressed carrier,

$$p_{\phi}(\phi) = \frac{\exp\left[\frac{\cos 2\phi}{4\sigma_{\phi}^2}\right]}{\int_{-\pi/2}^{\pi/2} \exp\left[\frac{\cos 2\psi}{4\sigma_{\phi}^2}\right] d\psi}, \quad |\phi| \leq \pi/2 \quad (\text{B-4})$$

For either case, $p_{\phi}(\phi)$ is assumed to be zero for $|\phi| > \pi/2$. The parameter σ_{ϕ}^2 is the carrier loop phase error variance. The presence of $f(\cdot)$ in equation (B-2) means that the HRM depends on the coding scheme; it also depends on the threshold BER.

The HRM radio loss for residual-carrier tracking has been evaluated by use of equations (B-1), (B-2) and (B-3); the results are shown in Figures 17 through 19. In those figures radio loss is given as a positive decibel quantity. That is to say, Figures 17 through 19 plot $-10 \log \eta_{HRM}$.

The HRM radio loss for suppressed-carrier tracking has been evaluated by use of equations (B-1), (B-2) and (B-4); the results are shown in Figures 20 through 22. In those figures radio loss is given as a positive decibel quantity. That is to say, Figures 20 through 22 plot $-10 \log \eta_{HRM}$.

Exponential approximations to the HRM are given in Table B-1. The parameter σ_{ϕ}^2 is, as before, the carrier loop phase error variance in units of rad^2 . The radio loss for the $(k=15, r=1/6)$ code is approximately the same as that for the $(k=15, r=1/4)$ code. The approximations of Table B-1 are valid for σ_{ϕ}^2 in the following range

$$\sigma_{\phi}^2 \leq \begin{cases} 0.1 \text{ rad}^2, & \text{Residual Carrier} \\ 0.02 \text{ rad}^2, & \text{Suppressed Carrier} \end{cases} \quad (\text{B-5})$$

If the computed radio loss is greater than 3.0 dB (i.e., if $-10 \log \eta_{HRM} > 3.0$), the result should not be trusted.

When there is a static phase error ξ_{spe} caused by doppler dynamics, $p_{\phi}(\phi)$ has a different form. For a residual-carrier loop

$$p_{\phi}(\phi) = \frac{\exp\left[\frac{\cos \phi + \phi \sin \xi_{spe}}{\sigma_{\phi}^2}\right]}{\int_{-\pi/2}^{\pi/2} \exp\left[\frac{\cos \psi + \psi \sin \xi_{spe}}{\sigma_{\phi}^2}\right] d\psi}, \quad |\phi| \leq \pi/2 \quad (\text{B-6})$$

B.2 *Low-Rate Model (LRM)*

The LRM is strictly valid only for extremely low symbol rates, namely when the symbol rate is much less than the carrier loop bandwidth, which is rarely the case in practice. The real value of the LRM is its use in the interpolation scheme of the MRM to help tame the pessimism of the HRM for relatively low symbol rates. The LRM is independent of the code and the threshold BER, so it is a much simpler theory than the HRM. The LRM radio loss, η_{LRM} (fractional and dimensionless), is given by

$$\eta_{LRM} = \left[\int_{-\pi/2}^{\pi/2} \cos \phi p_{\phi}(\phi) d\phi \right]^2 \quad (B-7)$$

where $p_{\phi}(\phi)$ is the probability density function of the carrier loop phase error ϕ .

The LRM radio loss for residual-carrier tracking is defined by equations (B-7) and (B-3). The LRM radio loss for suppressed-carrier tracking is defined by equations (B-7) and (B-4). Exponential approximations to the LRM are given in Table B-2. The parameter σ_{ϕ}^2 is, as before, the carrier loop phase error variance in units of rad^2 . The approximations of Table B-2 are valid for σ_{ϕ}^2 in the range defined by inequality (B-5).

Table B-2: LRM Radio Loss (dB) $= -10 \log \eta_{LRM} = c_0 (e^{c_1 \sigma_{\phi}^2} - 1)$

| Tracking Mode | Radio Loss Coefficient c_0 | Radio Loss Coefficient c_1 |
|------------------|---------------------------------|---------------------------------|
| Residual | 4.0 | 1.1 |
| Suppressed | 0.56 | 7.3 |

B.3 *Medium-Rate Model*

In general, radio loss can most accurately be modeled by an interpolation between the HRM and LRM. This interpolation, the MRM, is

$$\eta_{MRM} = a\eta_{HRM} + (1-a)\eta_{LRM} \quad (B-8)$$

where η_{MRM} is the MRM (fractional and dimensionless) estimate of radio loss and a is the interpolation factor given by

$$a = \frac{1}{4B_L T_{SYM}} \left[1 - \frac{1}{8B_L T_{SYM}} (1 - e^{-8B_L T_{SYM}}) \right] \quad (B-9)$$

Table B-1: HRM Radio Loss (dB) $= -10 \log \eta_{HRM} = c_0 (e^{c_1 \sigma_\phi^2} - 1)$

| Tracking Mode | Code | Threshold BER | Radio Loss Coefficient c_0 | Radio Loss Coefficient c_1 |
|---------------|---------------------|--------------------|------------------------------|------------------------------|
| Residual | uncoded | 10^{-2} | 0.53 | 8.1 |
| Residual | uncoded | 5×10^{-3} | 0.39 | 10.5 |
| Residual | uncoded | 10^{-3} | 0.21 | 17.5 |
| Residual | uncoded | 10^{-4} | 0.070 | 35.2 |
| Residual | uncoded | 10^{-5} | 0.030 | 55.5 |
| Suppressed | uncoded | 10^{-2} | 0.27 | 15.2 |
| Suppressed | uncoded | 5×10^{-3} | 0.21 | 18.5 |
| Suppressed | uncoded | 10^{-3} | 0.12 | 29.3 |
| Suppressed | uncoded | 10^{-4} | 0.031 | 62.7 |
| Suppressed | uncoded | 10^{-5} | 0.000023 | 244. |
| Residual | $(k = 7, r = 1/2)$ | 10^{-2} | 0.30 | 17.7 |
| Residual | $(k = 7, r = 1/2)$ | 5×10^{-3} | 0.24 | 21.6 |
| Residual | $(k = 7, r = 1/2)$ | 10^{-3} | 0.21 | 28.7 |
| Residual | $(k = 7, r = 1/2)$ | 10^{-4} | 0.11 | 45.8 |
| Residual | $(k = 7, r = 1/2)$ | 10^{-5} | 0.066 | 64.7 |
| Suppressed | $(k = 7, r = 1/2)$ | 10^{-2} | 0.11 | 34.6 |
| Suppressed | $(k = 7, r = 1/2)$ | 5×10^{-3} | 0.085 | 42.5 |
| Suppressed | $(k = 7, r = 1/2)$ | 10^{-3} | 0.041 | 65.2 |
| Suppressed | $(k = 7, r = 1/2)$ | 10^{-4} | 0.010 | 116. |
| Suppressed | $(k = 7, r = 1/2)$ | 10^{-5} | 0.0030 | 174. |
| Residual | $(k = 15, r = 1/4)$ | 10^{-2} | 0.45 | 16.6 |
| Residual | $(k = 15, r = 1/4)$ | 5×10^{-3} | 0.45 | 18.8 |
| Residual | $(k = 15, r = 1/4)$ | 10^{-3} | 0.34 | 27.3 |
| Residual | $(k = 15, r = 1/4)$ | 10^{-4} | 0.21 | 43.1 |
| Residual | $(k = 15, r = 1/4)$ | 10^{-5} | 0.13 | 61.5 |
| Suppressed | $(k = 15, r = 1/4)$ | 10^{-2} | 0.13 | 38.4 |
| Suppressed | $(k = 15, r = 1/4)$ | 5×10^{-3} | 0.098 | 46.9 |
| Suppressed | $(k = 15, r = 1/4)$ | 10^{-3} | 0.067 | 65.4 |
| Suppressed | $(k = 15, r = 1/4)$ | 10^{-4} | 0.044 | 93.4 |
| Suppressed | $(k = 15, r = 1/4)$ | 10^{-5} | 0.021 | 135. |

In equation (B-9) B_L is the (one-sided, noise-equivalent) carrier loop bandwidth and T_{SYM} is the symbol period (the reciprocal of symbol rate). The parameters η_{HRM} and η_{LRM} appearing in equation (B-7) are dimensionless fractions. If Tables B-1 and B-2 are used to estimate the HRM and LRM radio losses, the positive decibel quantities must first be converted to the dimensionless fractions η_{HRM} and η_{LRM} before equation (B-8) is used.

Appendix C Static Phase Error

The Block-V Receiver, with either a type 2 or type 3 loop, has a very large tracking range; even a Doppler offset of several megahertz can be tracked. With a finite Doppler rate, however, there will be a static phase error in a type 2 loop.

Table C-1 shows the static phase error in the carrier loop of the Block-V Receiver that results from various Doppler dynamics for several different loops. These equations are based on the work reported in Reference 10. The Doppler dynamics are here defined by the parameters α and β . B_L is the (one-sided) noise-equivalent loop bandwidth of the carrier loop.

$$\alpha = \text{Doppler Rate (Hz/s)} \quad (C-1)$$

$$\beta = \text{Doppler Acceleration (Hz/s}^2\text{)} \quad (C-2)$$

The equations of Table C-1 are valid for either residual-carrier or suppressed-carrier (Costas loop) operation of the Block-V Receiver. In the presence of a persistent Doppler acceleration, a type 2 loop will periodically slip cycles.

Table C-1: Static Phase Error (rad) for Block-V Receiver

| | Constant Range- Rate | Constant Derivative of Range-Rate | Constant Second Derivative of Range-Rate |
|--------------------------------------|-------------------------------|-----------------------------------------|------------------------------------------------------------------------------|
| Loop | Constant Doppler Offset | Constant Doppler Rate | Constant Doppler Acceleration |
| ----- | ----- | ----- | ----- |
| type 2, standard underdamped | 0 | $\frac{9\pi}{16B_L^2} \cdot \alpha$ | $\left(\frac{9\pi\beta}{16B_L^2} \right) t - \frac{27\pi\beta}{64B_L^3}$ |
| type 2, supercritically damped | 0 | $\frac{25\pi}{32B_L^2} \cdot \alpha$ | $\left(\frac{25\pi\beta}{32B_L^2} \right) t - \frac{125\pi\beta}{128B_L^3}$ |
| type 3, standard underdamped | 0 | 0 | $\frac{12167\pi}{8000B_L^3} \cdot \beta$ |
| type 3, supercritically damped | 0 | 0 | $\frac{35937\pi}{16384B_L^3} \cdot \beta$ |

Appendix D Transmitter Phase Noise

Transmitter phase noise contributes to the phase error in the receiver's carrier loop. This contribution is a zero-mean random process, and its variance equals

$$\sigma_\phi^2 = \int_0^\infty S_\theta(f) |1 - H(f)|^2 df \quad \text{rad}^2 \quad (\text{D-1})$$

where $S_\theta(f)$ is the one-sided power spectral density of the transmitter phase noise and $H(f)$ is the phase transfer function of the carrier loop. $S_\theta(f)$, with units of rad^2/Hz , is related to $L_\theta(f)$, the ratio (in decibels) of the modulation sideband power spectral density to the residual carrier power (Reference 11).

$$L_{\theta}(f) = 10 \log \left(\frac{1}{2} S_{\theta}(f) \right) \quad (\text{D-2})$$

Table D-1 lists approximate solutions to equation (D-1) for several types of carrier loop and for two types of phase noise. The approximate expressions of this table are valid for the Block-V Receiver tracking either a residual carrier or a suppressed carrier. B_L is the (one-sided) noise-equivalent carrier loop bandwidth.

Table D-1: Carrier Phase Error Variance, σ_{ϕ}^2 (rad²)

| | type 2 standard underdamped | type 2 supercritically damped | type 3 standard underdamped | type 3 supercritically damped |
|-----------------------------------|-----------------------------------|-------------------------------------|-----------------------------------|-------------------------------------|
| $S_{\theta}(f) = \frac{S_2}{f^2}$ | $\frac{3.7}{B_L} S_2$ | $\frac{3.0}{B_L} S_2$ | $\frac{4.5}{B_L} S_2$ | $\frac{3.8}{B_L} S_2$ |
| $S_{\theta}(f) = \frac{S_3}{f^3}$ | $\frac{8.7}{B_L^2} S_3$ | $\frac{7.7}{B_L^2} S_3$ | $\frac{12.8}{B_L^2} S_3$ | $\frac{10.5}{B_L^2} S_3$ |

For example, if the transmitter phase noise is flicker-of-frequency (i.e., $L_{\theta}(f)$ decreases with Fourier frequency f at a rate of 30 decibels per decade) in the frequency range of interest, and if $L_{\theta}(1 \text{ Hz}) = -45 \text{ dBc/Hz}$, then $S_{\theta}(f)$ may be modeled as S_3/f^3 with S_3 given by $2 \times 10^{-45/10} = 0.000063$.

Appendix E Solar Phase Noise

When the sun-earth-probe angle is small and the spacecraft is beyond the sun, microwave carriers pick up phase scintillations in passing through the solar corona. There is a resulting contribution to phase error in the carrier loop. The magnitude of the effect is highly variable, depending on the activity of the sun. Equation (E-1) below, based on the work reported in Reference 12, offers a coarse estimate of the average solar contribution, in units of rad², to carrier loop phase error variance. It is valid for the Block-V Receiver tracking either a residual carrier or a suppressed carrier and for sun-earth-probe angles between 5° and 27°.

$$\sigma_s^2 = \frac{C_{band} \cdot C_{loop}}{(\sin \beta)^{2.45} \cdot B_L^{1.65}}, \quad 5^\circ \leq \beta \leq 27^\circ \quad (\text{E-1})$$

In equation (E-1) β is the sun-earth-probe angle and B_L is the (one-sided) noise-equivalent carrier loop bandwidth. C_{band} is a constant for a given set of operating bands. For one-way or two-way noncoherent operation,

$$C_{band} = \begin{cases} 2.6 \times 10^{-5}, & \text{S-down} \\ 1.9 \times 10^{-6}, & \text{X-down} \end{cases} \quad (\text{E-2})$$

For two-way coherent operation,

$$C_{band} = \begin{cases} 6.1 \times 10^{-5}, & \text{S-up / S-down} \\ 4.8 \times 10^{-4}, & \text{S-up / X-down} \\ 5.5 \times 10^{-6}, & \text{X-up / X-down} \end{cases} \quad (\text{E-3})$$

C_{loop} is a constant for a given carrier loop.

$$C_{loop} = \begin{cases} 5.9, & \text{standard underdamped type 2 loop} \\ 5.0, & \text{supercritically damped type 2 loop} \\ 8.2, & \text{standard underdamped type 3 loop} \\ 6.7, & \text{supercritically damped type 3 loop} \end{cases} \quad (\text{E-4})$$

Appendix F Subcarrier Demodulation Loss

The subcarrier demodulation loss η_{SUB} (fractional and dimensionless) is

$$\eta_{SUB} = \frac{f^{-1}(\text{BER})}{E_b/N_0} \quad (\text{F-1})$$

where $f(\cdot)$ is the ideal functional dependence of probability of bit error on bit SNR (see Appendix A), corresponding to zero decibels of system loss. In equation (F-1) E_b/N_0 is the actual bit SNR needed to achieve a given threshold BER in the presence of imperfect subcarrier synchronization (with the assumption of perfect carrier and symbol synchronization); in the case of a squarewave subcarrier, it is the solution of the following equation

$$\text{BER} = \int_{-\pi/2}^{\pi/2} f\left(\frac{E_b}{N_0} \left[1 - \frac{2}{\pi} |\phi|\right]^2\right) p_\phi(\phi) d\phi \quad (\text{F-2})$$

where BER is, as before, the threshold bit error rate. The probability density function $p_\phi(\phi)$ of squarewave subcarrier loop phase error ϕ is modeled as having a Gaussian form within the limits $|\phi| \leq \pi/2$ and as zero outside those limits.

$$p_{\phi}(\phi) = \frac{\exp(-\rho_{SUB}\phi^2/2)}{\int_{-\pi/2}^{\pi/2} \exp(-\rho_{SUB}\psi^2/2) d\psi} \quad (F-3)$$

where ρ_{SUB} is the squarewave subcarrier loop signal-to-noise ratio as computed from equation (27). Equations (F-1), (F-2) and (F-3) define the subcarrier demodulation loss model for a squarewave subcarrier. The presence of $f(\cdot)$ in equation (F-2) means that the subcarrier demodulation loss depends on the coding scheme; it also depends on the threshold BER. The squarewave subcarrier demodulation loss is shown in Figures 24 through 26. In those figures subcarrier demodulation loss is given as a positive decibel quantity. That is to say, Figures 24 through 26 plot $-10 \log \eta_{SUB}$. Exponential approximations to the squarewave subcarrier demodulation loss are given in Table F-1. The subcarrier demodulation loss for the $(k=15, r=1/6)$ code is approximately the same as that for the $(k=15, r=1/4)$ code.

Table F-1: Squarewave Subcarrier Demodulation Loss (dB) = $-10 \log \eta_{SUB} = c_0 (\rho_{SUB})^{c_1}$,
where ρ_{SUB} is the dimensionless signal-to-noise ratio in a squarewave
subcarrier loop.

| Code | Threshold BER | Subcarrier Demodulation Loss Coefficient c_0 | Subcarrier Demodulation Loss Coefficient c_1 |
|-----------------|--------------------|------------------------------------------------------|------------------------------------------------------|
| uncoded | 10^{-2} | 6.3 | -0.55 |
| uncoded | 5×10^{-3} | 6.6 | -0.56 |
| uncoded | 10^{-3} | 7.7 | -0.58 |
| uncoded | 10^{-4} | 9.8 | -0.61 |
| uncoded | 10^{-5} | 13. | -0.66 |
| $(k=7, r=1/2)$ | 10^{-2} | 12. | -0.65 |
| $(k=7, r=1/2)$ | 5×10^{-3} | 13. | -0.66 |
| $(k=7, r=1/2)$ | 10^{-3} | 16. | -0.69 |
| $(k=7, r=1/2)$ | 10^{-4} | 21. | -0.74 |
| $(k=7, r=1/2)$ | 10^{-5} | 29. | -0.78 |
| $(k=15, r=1/4)$ | 10^{-2} | 22. | -0.73 |
| $(k=15, r=1/4)$ | 5×10^{-3} | 25. | -0.76 |
| $(k=15, r=1/4)$ | 10^{-3} | 31. | -0.79 |
| $(k=15, r=1/4)$ | 10^{-4} | 40. | -0.83 |
| $(k=15, r=1/4)$ | 10^{-5} | 53. | -0.87 |

For a sinewave subcarrier, the subcarrier demodulation loss is governed by equations (B-1), (B-2) and (B-4), which also characterize the HRM radio loss with suppressed carrier, except that σ_ϕ^2 is replaced by $1/\rho_{SUB}$, where ρ_{SUB} is the sinewave subcarrier signal-to-noise ratio as defined in equation (27). Exponential approximations to the sinewave subcarrier demodulation loss are given in Table F-2. The subcarrier demodulation loss for the $(k = 15, r = 1/6)$ code is approximately the same as that for the $(k = 15, r = 1/4)$ code.

The approximations of Table F-1 and Table F-2 are valid for ρ_{SUB} in the following range

$$\rho_{SUB} \geq \begin{cases} 100.0 \text{ (20 dB),} & \text{squarewave subcarrier} \\ 50.0 \text{ (17 dB),} & \text{sinewave subcarrier} \end{cases} \quad (\text{F-4})$$

Table F-2: Sinewave Subcarrier Demodulation Loss (dB) = $-10\log\eta_{SUB} = c_0(e^{c_1/\rho_{SUB}} - 1)$,
where ρ_{SUB} is the dimensionless signal-to-noise ratio in a sinewave subcarrier loop.

| Code | Threshold BER | Subcarrier Demodulation Loss Coefficient c_0 | Subcarrier Demodulation Loss Coefficient c_1 |
|---------------------|--------------------|------------------------------------------------------|------------------------------------------------------|
| ----- | ----- | ----- | ----- |
| uncoded | 10^{-2} | 0.27 | 15.2 |
| uncoded | 5×10^{-3} | 0.21 | 18.5 |
| uncoded | 10^{-3} | 0.12 | 29.3 |
| uncoded | 10^{-4} | 0.031 | 62.7 |
| uncoded | 10^{-5} | 0.000023 | 244. |
| $(k = 7, r = 1/2)$ | 10^{-2} | 0.11 | 34.6 |
| $(k = 7, r = 1/2)$ | 5×10^{-3} | 0.085 | 42.5 |
| $(k = 7, r = 1/2)$ | 10^{-3} | 0.041 | 65.2 |
| $(k = 7, r = 1/2)$ | 10^{-4} | 0.010 | 116. |
| $(k = 7, r = 1/2)$ | 10^{-5} | 0.0030 | 174. |
| $(k = 15, r = 1/4)$ | 10^{-2} | 0.13 | 38.4 |
| $(k = 15, r = 1/4)$ | 5×10^{-3} | 0.098 | 46.9 |
| $(k = 15, r = 1/4)$ | 10^{-3} | 0.067 | 65.4 |
| $(k = 15, r = 1/4)$ | 10^{-4} | 0.044 | 93.4 |
| $(k = 15, r = 1/4)$ | 10^{-5} | 0.021 | 135. |

Appendix G *Symbol Loop Squaring Loss*

Symbol loop squaring loss S_{SYM} is given by (Reference 8)

$$S_{SYM} = \frac{\left[\operatorname{erf}\left(\sqrt{E_s/N_0}\right) - \frac{W_{SYM}}{2} \sqrt{\frac{E_s/N_0}{\pi}} \exp(-E_s/N_0) \right]^2}{1 + \frac{W_{SYM}}{2} E_s/N_0 - \frac{W_{SYM}}{2} \left[\frac{1}{\sqrt{\pi}} \exp(-E_s/N_0) + \sqrt{E_s/N_0} \operatorname{erf}\left(\sqrt{E_s/N_0}\right) \right]^2} \quad (\text{G-1})$$

where the error function is given by

$$\operatorname{erf}(x) = \frac{2}{\sqrt{\pi}} \int_0^x e^{-y^2} dy \quad (\text{G-2})$$

Appendix H *Symbol Synchronization Loss*

The symbol synchronization loss η_{SYM} (fractional and dimensionless) is

$$\eta_{SYM} = \frac{f^{-1}(\text{BER})}{E_b/N_0} \quad (\text{H-1})$$

where $f(\cdot)$ is the ideal functional dependence of probability of bit error on bit SNR (see Appendix A), corresponding to zero decibels of system loss. In equation (H-1) E_b/N_0 is the actual bit SNR needed to achieve a given threshold BER in the presence of imperfect symbol synchronization (with the assumption of perfect carrier and subcarrier synchronization); it is the solution of the following equation

$$\text{BER} = \int_{-\pi/2}^{\pi/2} f\left(\frac{E_b}{N_0} \left[\frac{1}{2} \left\{ 1 + \left(1 - \frac{|\phi|}{\pi} \right)^2 \right\} \right]\right) p_\phi(\phi) d\phi \quad (\text{H-2})$$

where BER is, as before, the threshold bit error rate. The probability density function $p_\phi(\phi)$ of symbol loop phase error ϕ is modeled as having a Gaussian form within the limits $|\phi| \leq \pi/2$ and as zero outside those limits.

$$p_\phi(\phi) = \frac{\exp(-\rho_{SYM} \phi^2 / 2)}{\int_{-\pi/2}^{\pi/2} \exp(-\rho_{SYM} \psi^2 / 2) d\psi} \quad (\text{H-3})$$

In equation (H-3) ρ_{SYM} is the symbol loop signal-to-noise ratio as computed from equation (30). Equations (H-1), (H-2) and (H-3) define the symbol synchronization loss model. The symbol synchronization loss is shown in Figure 28, where it is represented as a positive decibel quantity. That is to say, Figure 28 plots $-10 \log \eta_{SYM}$. While in principle η_{SYM} should depend on the coding scheme and the threshold BER, in fact η_{SYM} is approximately the same for all coding schemes and threshold BERs of interest. A simple exponential approximation is

$$-10 \log \eta_{SYM} = 2.5(\rho_{SYM})^{-0.65} \text{ dB} \quad (\text{H-4})$$

where ρ_{SYM} is the dimensionless signal-to-noise ratio in the symbol loop as computed from equation (30). This approximation is valid for ρ_{SYM} in the following range

$$\rho_{SYM} \geq 31.6 \text{ (15 dB)} \quad (\text{H-5})$$

Appendix I References

1. J. B. Berner and K. M. Ware, "An Extremely Sensitive Digital Receiver for Deep Space Satellite Communications," *Eleventh Annual International Phoenix Conference on Computers and Communications*, pp. 577-584, Scottsdale, Arizona, April 1-3, 1992.
2. J. P. Costas, "Synchronous Communications," *Proceedings of the IRE*, Vol. 44, pp. 1713-1718, December 1956.
3. M. Aung, W. J. Hurd, C. M. Buu, J. B. Berner, S. A. Stephens, and J. M. Gevargiz, "The Block V Receiver Fast Acquisition Algorithm for the Galileo S-Band Mission," *TDA Progress Report 42-118*, pp. 83-114, August 15, 1994.
4. J. Lesh, "Tracking Loop and Modulation Format Considerations for High Rate Telemetry," *DSN Progress Report 42-44*, pp. 117-124, April 15, 1978.
5. M. K. Simon and W. C. Lindsey, "Optimum Performance of Suppressed Carrier Receivers with Costas Loop Tracking," *IEEE Transactions on Communications*, Vol. COM-25, No. 2, pp. 215-227, February 1977.
6. L. C. Palmer and S. A. Klein, "Phase Slipping in Phase-Locked Loop Configurations That Track Biphase or Quadriphase Modulated Carriers," *IEEE Transactions on Communications*, pp. 984-991, October 1972.
7. W. J. Hurd and S. Aguirre, "A Method to Dramatically Improve Subcarrier Tracking," *TDA Progress Report 42-86*, pp. 103-110, August 15, 1986.

8. M. Aung, "Tracking Performance and Cycle Slipping in the All-Digital Symbol Synchronizer Loop of the Block V Receiver," *TDA Progress Report 42-111*, pp. 179-191, November 15, 1992.
9. J. H. Yuen, editor, *Deep Space Telecommunications Systems Engineering*, Plenum Press, New York, 1983.
10. S. A. Stephens and J. B. Thomas, "Controlled-Root Formulation for Digital Phase-Locked Loops," *IEEE Transactions on Aerospace and Electronic Systems*, Vol. 31, No. 1, pp. 78-95, January 1995.
11. D. Halford, J. H. Shoaf, and A. S. Risley, "Spectral Density Analysis: Frequency Domain Specification and Measurement of Signal Stability," *Proceedings of the 27th Annual Symposium on Frequency Control 1973*, Cherry Hill, New Jersey, 1973, pp. 421-431. (Also published as *NBS Technical Note 632*.)
12. R. Woo and J. W. Armstrong, "Spacecraft Radio Scattering Observations of the Power Spectrum of Electron Density Fluctuations in the Solar Wind," *Journal of Geophysical Research*, Vol. 84, No. A12, pp. 7288-7296, December 1, 1979.